NTNU
Norwegian University of
Science and Technology

Investigation of the Seebeck Effect and the Soret Effect in Ionic Systems Using Molecular Dynamics

Kristine Veie

Chemical Engineering and Biotechnology
Submission date: June 2018
Supervisor: Bjørn Hafskjold, IKJ
Co-supervisor: Signe Kjelstrup, IKJ

Norwegian University of Science and Technology
Department of Chemistry

Summary

Molecular dynamics simulations were performed in order to investigate the Soret and Seebeck effect in an electrolyte solution consisting of LiCl and water. A pure water system was also constructed in order to study the orientation of the water molecules when a thermal gradient is applied, and the electric field and the thermopolarization coefficient were calculated. In order to investigate if the contribution from the ions to the Seebeck effect in the electrolyte solution depends on the water molecules, a system consisting of LiCl was constructed, where the dielectric constant for water was used. The diffusion coefficients for water, lithium, and chloride were calculated, in addition to the thermal conductivities for the systems.

The electric field and the thermopolarization coefficient in the pure water system are in good agreement with the results obtained by Armstrong and Bresme [1]. The electric field was calculated from two methods: by integrating the charge density and by summing the di- and quadrupole contributions to the field. According to Armstrong and Bresme, the methods should yield the same result [1]. In this thesis, the two methods were in agreement within the statistical error. From the sign of the dipolar contribution to the electric field, it was concluded that the dipole moment of water points towards the hot side of the simulation box.

For the electrolyte solution, the two methods for calculating the electric field did not yield the same result. Within the statistical errors calculated in this thesis, the results are not equal to the results obtained by Lecce and Bresme [2]. When the field was calculated by integrating the charge density, the Seebeck coefficient was equal to (-8$\pm$3)$\cdot 10^{-4}$ V K^{-1}. The coefficient calculated by Lecce and Bresme is approximately equal to -3$\cdot 10^{-4}$ V K^{-1} [2]. Since Lecce and Bresme did not give the standard deviation of the coefficient, it is difficult to say how different the results are, but the coefficients have the same sign and order of magnitude. In this thesis, both of the methods for calculating the electric field yielded a positive ion contribution and a negative water contribution, and this is in agreement with Lecce and Bresme's results. The pressure in this system and the system size were different from what Lecce and Bresme used, and this could have influenced the results. The results in this thesis indicate that the Seebeck effect is a sensitive effect. The Soret coefficient calculated for the electrolyte solution is in good agreement with the coefficient calculated by Lecce and Bresme, given in [2].

In the system consisting of LiCl, where the dielectric constant for water was used, the calculated Seebeck coefficient differed from the one calculated for the electrolyte solution. This indicates that the ion contribution to the Seebeck coefficient in the electrolyte solution depends on the water molecules.

Sammendrag

Ved hjelp av molekyldynamikksimuleringer ble Soret og Seebeck effekten undersøkt i en elektrolyttløsning bestående av LiCl og vann. I tillegg ble et system bestående av rent vann laget for å undersøke orienteringen av vannmolekylene når en temperaturgradient er tilstede, og det elektriske feltet og termopolariseringskoeffisienten ble også beregnet. For å undersøke om ionebidraget til Seebeck effekten i elektrolyttløsningen er avhengig av vannmolekylene tilstede, ble det laget et system bestående av LiCl, hvor den dielektriske konstanten for vann ble brukt. Det ble i tillegg beregnet diffusjonskoeffisienter for rent vann og i elektrolyttløsningen, samt den termiske ledningsevnen til de to systemene.

Det elektriske feltet og termopolariseringskoeffisienten beregnet i denne oppgaven er i godt samsvar med resultatene til Armstrong og Bresme [1]. Det elektriske feltet ble beregnet fra to ulike metoder: ved å integrere ladningstettheten og ved å summere de dipolare og quadrupolare bidragene til det elektriske feltet. I følge Armstrong og Bresme, så skal de to metodene gi det samme resultatet [1]. I denne oppgaven ga de to metodene det samme resultatet for det elektriske feltet. Fra fortegnet på det dipolare bidraget til det elektriske feltet ble det konkludert med at dipolmomentet til vann peker mot den varme siden av simuleringsboksen.

For elektrolyttløsningen så ga ikke de to metodene for å beregne det elektriske feltet det samme resultatet. Innenfor standardavvikene beregnet i denne oppgaven gir ingen av de to metodene likt resultat som det Lecce og Bresme har beregnet [2]. Da det elektriske feltet ble beregnet ved å integrere ladningstettheten, ble den resulterende Seebeck koeffisienten lik (-8$\pm$3)$\cdot 10^{-4}$ V K^{-1}. Lecce og Bresme beregnet en koeffisient omtrent lik -3$\cdot 10^{-4}$ V K^{-1} [2]. Siden Lecce og Bresme ikke inkluderte standardavviket i sine resultater, er det vanskelig å si hvor forskjellig resultatet i denne oppgaven er fra deres, men både størrelsesorden og fortegn er i samsvar. Begge metodene for beregningen av det elektriske feltet ga et positivt ionebidrag og et negativt bidrag fra vann til det elektriske feltet. Dette er i samsvar med Lecce og Bresmes resultater [2]. Trykket i dette systemet og systemstørrelsen var litt ulikt fra hva Lecce og Bresme brukte, og dette kan ha påvirket resultatet. Resultatene i denne masteroppgaven indikerer at Seebeck effekten er en sensitiv effekt. Soret koeffisienten beregnet for elektrolyttløsningen samsvarer med koeffisienten som Lecce og Bresme beregnet [2].

Seebeck koeffisienten ble også beregnet i systemet bestående av LiCl, hvor den dielektriske konstanten for vann ble brukt. Den beregnede koeffisienten var forskjellig fra den som ble beregnet for elektrolyttløsningen. Dette indikerer at ionebidraget til Seebeck koeffisienten i elektrolyttløsningen er avhengig av vannmolekylene.

Acknowledgements

I would like to thank my supervisors Bjørn Hafskjold and Signe Kjelstrup for all their help regarding my thesis, and for helpful discussions. During the work with my master's thesis, I had a short trip to Imperial College, so I would like to thank Fernando Bresme and his research group for hosting me. Fernando Bresme and I have had many useful discussions, both ahead of, during, and after my trip to London. I would also like to thank Dick Bedeaux for helpful feedback. Additionally, I would like to thank Olav Galteland, Sondre Schnell, and Anders Lervik for all their help regarding LAMMPS.

Many thanks to the other master students in my group, Laura Edvardsen and Vilde Bråten for helpful discussions and good collaboration.

I am also grateful to the NOTUR facilities for providing computational resources.

Contents

List of symbols

Symbol	Unit	Description
σ	J s^{-1} K^{-1} m^{-3}	Local entropy production
J_i	mol m^2 s^{-1}	Flux of component i
X_i		Thermodynamic driving force
L_{ij}		Phenomenological coefficient for coupling of fluxes i and j
J'_q	J m^2 s^{-1}	Flux of measurable heat
T	K	Temperature
J_j	mol m^2 s^{-1}	Flux of component j
$\mu_{j,T}$	J mol^{-1}	Chemical potential of j at constant T
j	A m^{-2}	Electric current density
ϕ	V	Electric potential
x		Coordinate
r	mol m^{-3} s^{-1}, ohm m^{-1}	Reaction rate, Ohmic resistivity
d	m	Thickness of layer
$\Delta_r G$	J mol^{-1}	Reaction Gibbs energy
S_E	V K^{-1}	Seebeck coefficient, without electrodes
η_E	V K^{-1}	Seebeck coefficient, with electrodes
$\Delta\phi$	V	Change in electric potential
S^*	J K^{-1} mol^{-1}	Transported entropy
S	J K^{-1} mol^{-1}	Thermodynamic entropy
F	C mol^{-1}	Faraday's constant
c	mol m^{-3}	Concentration
λ	W K^{-1} m^{-1}	Thermal conductivity
π	J	Peltier coefficient
κ	S m^{-1}	Electrical conductivity
J_v	J m^3 s^{-1}	Volume flux
p	bar	Pressure
L_p		Proportionality constant
Π_{xy}	bar	Viscous pressure tensor
η	bar s	Shear viscosity
v_x	m s^{-1}	Velocity in x-direction
ϵ_0	F m^{-1}	Vacuum permittivity

Symbol	Unit	Description
ϵ_r		Relative dielectric constant
ρ	C m^{-3}, g cm^{-3}	Charge density, density
E	V m^{-1}	Electric field
E_{eq}	V m^{-1}	Equilibrium electric field
P	C m^2	Polarization density
χ_e		Electric susceptibility
∇T	K m^{-1}	Gradient in temperature
E_M	V m^{-1}	Monopolar contribution to electric field
E_{P_x}	V m^{-1}	Dipolar contribution to electric field
$E_{Q_{xx}}$	V m^{-1}	Quadrupolar contribution to electric field
q_i	C	Charge of species i
R	J mol^{-1} K^{-1}	Gas constant
γ		Activity coefficient
μ_i°	J mol^{-1}	Chemical potential of pure i
μ_i	J mol^{-1}	Chemical potential of i
$D_{1,2}$	m^2 s^{-1} K^{-1}	Interdiffusion coefficient of component 1
D_T	m^2 s^{-1} K^{-1}	Thermal diffusion coefficient
s_T	K^{-1}	Soret coefficient
x_i		Mole fraction of component i
R	m	Distance
μ_x, μ_y, μ_z	C Å	Dipole vector in x-,y-,z-directions
q	C $Å^2$	Quadrupole moment
V	cm^{-3}	Volume
μ	m^2 V^{-1} s^{-1}	Ion mobility
v	m s^{-1}	Velocity
z		Charge number
m_i	kg	Mass of particle i
$\mathbf{f}_i$	N	Force acting on particle i
$\mathbf{r}_i$		Position of particle i
t	s	Time
N		Number of degrees of freedom
V	kcal mol^{-1}	Lennard Jones and Coulomb potential
ε	kcal mol^{-1}	Depth of potential well

Symbol	Unit	Description
σ	Å	The distance between two particles when LJ potential is 0
r	Å	Distance between two particles
D	$m^2\ s^{-1}$	Self diffusion coefficient
J_q	$J\ m^2\ s^{-1}$	Flux of total heat
e_i	$kcal\ mol^{-1}$	Per atom potential and kinetic energy
$\mathbf{v}_i$	Å fs^{-1}	Velocity of particle i
$\mathbf{S}_i$	$kcal\ mol^{-1}$	Per atom stress tensor
k_B	$J\ K^{-1}$	Boltzmann's constant
H	$J\ mol^{-1}$	Partial molar enthalpy
J_m	$mol\ m^2\ s^{-1}$	Mass flux of one component
$\pm\Delta u$	J	Energy added/subtracted (+/-) from hot/cold regions
δt	s	Time step
A	m^2	Cross sectional area of simulation box
S_{TP}	$V\ K^{-1}$	Thermopolarization coefficient
$\boldsymbol{e_x}$, $\boldsymbol{e_x}$		Unit vector in x-direction, dipole unit vector
$\cos(\theta_{\mu x})$		Cosine to the angle between the dipole vector and x-direction
M_m	$g\ mol^{-1}$	Molar mass

List of Figures

List of Tables

1 Introduction

In 1821 Thomas Johann Seebeck discovered that keeping the ends of a metal bar at different temperatures induced an electric current [5]. In one of his experiments he kept two electrically connected junctions at different temperatures and the wire connected to the junctions caused a compass needle to deflect. A few years later, Peltier discovered that a heat flux can be generated from an electric voltage difference [6]. This means that there is a coupling between transport of heat and charge, and thermocouples and thermoelectric heat pumps are examples of devices that exploit this coupling.

Charles Soret discovered in 1879 after studying a tube containing a salt solution that the salt composition did not remain uniform if the ends of the tube were kept at different temperatures [7]. He concluded that because of the presence of a temperature gradient, a mass flux of salt was generated. Carl Ludwig actually described the same phenomena a few years earlier and he formulated equations for describing the mass separation due to a temperature gradient. The coupling between heat and mass transfer is important in different processes, such as absorption, distillation extraction, melting, and crystallization [6].

Over the past 10-15 years, there have been a great interest of both the understanding and the performance of thermoelectric materials [8]. These materials can convert waste heat into useful electrical energy. Thermoelectric materials can also be used for refrigeration purposes. The conversion of waste heat into electrical energy is important for reducing the use of fossil fuels and for reducing the emissions from greenhouse gases.

Non-equilibrium thermodynamics is important in many processes within the fields of biology, physics, and materials science [9]. Because of the coupling among two or more fluxes, the introduction of a thermal gradient leads to non-equilibrium responses in the system [1]. F. Bresme, A. Lervik, D. Bedeaux and S. Kjelstrup discovered that thermal gradients can induce thermopolarization fields in water [10]. They used the Central Force Model to model water. They found that, in the presence of a thermal gradient, the water molecules reorient after the thermal field, thus leading to an electrostatic field. A few years later, Armstrong and Bresme quantified the same effect using the SPC/E water model [1]. Since water is one of the most important solvents in biology and materials science it is interesting and important to understand the response of water to thermal gradients.

One of the goals of this master's thesis is to reproduce some of the results obtained by Silvia Di Lecce and Fernando Bresme at Imperial College, London, given in [2]. Lecce and Bresme found that in an electrolyte solution, both the electric field for the ions and for water contributes to the total electric field and by that reason to the Seebeck coefficient. Lecce and

Bresme calculated a Seebeck coefficient equal to 25.7 μV K^{-1} at 298 K for the electrolyte solution consisting of LiCl and water. The Soret effect will also be studied in this electrolyte solution.

Another objective is to investigate if the contribution from the ions to the Seebeck effect in an electrolyte solution depends on the water molecules present in the solution. This will be investigated by comparing the electrolyte solution with a system consisting of only ions where the dielectric constant for water is used rather than including any actual water molecules.

A one-component system consisting of pure water will also be constructed, in order to study the orientation of the water molecules in presence of a temperature gradient. The electric field will also be computed, and the results will be compared to the results obtained by Jeff Armstrong and Fernando Bresme [1].

So this master's thesis is divided into two parts: the first part consists of reproducing some of the results obtained by Lecce and Bresme [2] and Armstrong and Bresme [1]. In the second part, the goal is to get a better understanding of the role of water in the electrolyte solution.

This thesis is structured as follows; in section 2 and 3, some theoretical and computational background are presented. The simulation method is described in section 4. In section 5, the results are presented and discussed. The conclusion is presented in section 6.

2 Theoretical background

In the following sections, some theoretical background is presented.

2.1 The entropy production

The second law of thermodynamics can be reformulated in terms of the entropy production, σ, and is given by [11]

$$\sigma = \sum_i J_i X_i \geq 0, \tag{2.1}$$

where σ is greater or equal to 0. J_i and X_i are the conjugate fluxes and forces in the system. J_i can be expressed as a linear combination of all forces,

$$J_i = \sum_j L_{ij} X_j \tag{2.2}$$

The Onsager reciprocal relations are defined as

$$L_{ji} = L_{ij} \tag{2.3}$$

The entropy production of a one-dimensional transport processes is given by [11]:

$$\sigma = J_q^{'} \left(\frac{\partial}{\partial x} \frac{1}{T} \right) + \sum_{j=1}^{n} J_j \left(-\frac{1}{T} \frac{\partial \mu_{j,T}}{\partial x} \right) + j \left(-\frac{1}{T} \frac{\partial \phi}{\partial x} \right) + r \left(-\frac{\Delta_r G}{T} \right), \tag{2.4}$$

where $J_q^{'}$ is the measurable heat flux, T is the temperature, J_j are the component fluxes, $\mu_{j,T}$ is the chemical potential of component j at constant T, j is the electric current density, $\frac{\partial \phi}{\partial x}$ is the gradient in electric potential, r is the reaction rate and $\Delta_r G$ is the reaction Gibbs energy.

The simplest equations for describing the transport of heat, mass, charge, and volume are the equations of Fourier, Fick, Ohm, Darcy, and Newton. Fourier's law expresses the measurable heat flux, $J_q^{'}$, as the thermal conductivity, λ, times a temperature gradient, $\frac{dT}{dx}$:

$$J_q^{'} = -\lambda \frac{dT}{dx} \tag{2.5}$$

The mass flux of one of the components, J, in a binary system is by Fick's law expressed as

$$J = -D\frac{dc}{dx}, \tag{2.6}$$

where D is the diffusion coefficient and dc/dx is the gradient in molar concentration. Ohm's law expresses the electric current, j, in terms of the electrical conductivity, κ, times the gradient in electric potential:

$$j = -\kappa\frac{d\phi}{dx} \tag{2.7}$$

The volume flow through a porous medium, J_v, can be described by Darcy's law, which states that J_v is proportional to the pressure gradient, with a proportionality constant equal to L_p:

$$J_v = -L_p\frac{dp}{dx} \tag{2.8}$$

Newton's law of friction states that the viscous pressure tensor is proportional to the gradient in velocity, with a proportionality constant equal to η, which is the shear viscosity:

$$\Pi_{xy} = \eta\frac{\partial v_x}{\partial y} \tag{2.9}$$

Each of the fluxes in equation (2.5)-(2.9) have only one driving force. By using non-equilibrium thermodynamics, these equations can be generalized by taking all driving forces into account, and show that the transport equations are connected. If there is mass transport in a system, a gradient in chemical potential can be present, but also a gradient in temperature or electrical potential. In other words, non-equilibrium thermodynamics show that there is a coupling among fluxes.

The linear relations for the fluxes in equation (2.5)-(2.7) can be written as:

$$J_q^{'} = L_{qq}\frac{d}{dx}\left(\frac{1}{T}\right) + L_{q\mu}\left(-\frac{1}{T}\frac{\mu_T}{dx}\right) + L_{q\phi}\left(-\frac{1}{T}\frac{d\phi}{dx}\right) \tag{2.10}$$

$$J = L_{\mu q}\frac{d}{dx}\left(\frac{1}{T}\right) + L_{\mu\mu}\left(-\frac{1}{T}\frac{\mu_T}{dx}\right) + L_{\mu\phi}\left(-\frac{1}{T}\frac{d\phi}{dx}\right) \tag{2.11}$$

$$j = L_{\phi q}\frac{d}{dx}\left(\frac{1}{T}\right) + L_{\phi\mu}\left(-\frac{1}{T}\frac{\mu_T}{dx}\right) + L_{\phi\phi}\left(-\frac{1}{T}\frac{d\phi}{dx}\right) \tag{2.12}$$

The conjugate force of transport to $J_q^{'}$ is the thermal force $\frac{d(1/T)}{dx}$, for J it is the chemical force $[-\frac{1}{T}\frac{d\mu_T}{dx}]$ and for j it is the electrical force $[-\frac{1}{T}\frac{d\phi}{dx}]$.

The following are the Onsager relations:

$$L_{\mu q} = L_{q\mu}, \quad L_{q\phi} = L_{\phi q}, \quad L_{\phi\mu} = L_{\mu\phi} \tag{2.13}$$

The Onsager coefficients must be measured. The coefficients on the diagonal of the matrix are called the main coefficients, and the coupling coefficients are the off-diagonal coefficients. The coupling coefficients describe the coupling between the fluxes.

2.2 The Seebeck effect

The Seebeck effect is the phenomenon when a voltage difference is produced in presence of a temperature gradient [6]. The Seebeck coefficient is a function of transported entropy and thermodynamic entropy, and the expression for the Seebeck coefficient is individual for different types of cells. In this thesis, there are no electrodes present. In an experiment, if the Seebeck coefficient is to be measured, the electrodes are present. In the next 2 pages, the expression for the Seebeck coefficient for an experimental situation will be derived. This is done to illustrate that the expression for the Seebeck coefficient is different when the electrodes are present, compared to when they are not present. Next, the expression used in this thesis, when no electrodes are present, will be derived. Some comments of the differences between the two expressions for the Seebeck coefficient then follows.

An example cell, with electrodes, is the following [6]:

$$T^l, Mo(s)|Pb(l)|PbCl_2(l), MCl(l)|Pb(l)|Mo(s), T^r \tag{2.14}$$

In the cell described in equation (2.14), the electrodes consists of liquid lead and the electrolyte consists of two different molten salts. Mo-wires connects the electrodes to a potentiometer. T^l and T^r are the left and right temperatures, respectively. The cell can be divided into five homogeneous phases, denoted l, a, e, c and r. The interfaces between the homogeneous phases are denoted (s,l), (s,a), (s,c) and (s,r).

The Seebeck coefficient, η_E, is given by [6]:

$$\eta_E = \left(\frac{\Delta_{tot}\phi}{\Delta T} \right)_{j=0}, \tag{2.15}$$

where $\Delta_{tot}\phi$ is the total cell potential and ΔT is the temperature difference across the cell. The goal is to express the Seebeck coefficient in equation (2.15) in terms of the transported entropies and the thermodynamic entropies. In order to do that, the entropy production, σ, in the metal phases needs to be defined:

$$\sigma = J_q^{'} \left(\frac{\partial}{\partial T} \frac{1}{T} \right) + j \left(-\frac{1}{T} \frac{\partial \phi}{\partial x} \right), \tag{2.16}$$

where $J_q^{'}$ is the measurable heat flux, T is the temperature and $\frac{\partial \phi}{\partial x}$ is the electric potential gradient.

The equations for the temperature gradient and the electric potential gradient are given by:

$$\frac{\partial T}{\partial x} = -\frac{1}{\lambda} \left(J_q^{'} - \pi \frac{j}{F} \right) \tag{2.17}$$

$$\frac{\partial \phi}{\partial x} = -\frac{\pi}{TF} \frac{\partial T}{\partial x} - rj, \tag{2.18}$$

where λ is the stationary state thermal conductivity, π is the Peltier coefficient, F is Faraday's constant, r is the resistivity, and j is the electric current density.

The reciprocal effect of the Seebeck effect is the Peltier effect, which means that heat is transported due to a voltage gradient. The Peltier coefficient, π, can be defined in terms of transported entropy, S^*, and the Peltier coefficients for the Mo phase and the anode and cathode phases are:

$$\pi^l = \pi^r = T S^*_{e-,Mo} \tag{2.19}$$

$$\pi^a = \pi^c = T S^*_{e-,Pb} \tag{2.20}$$

The next step is to find an expression for the total cell potential, $\Delta_{tot}\phi$. This expression is found by summing all the contributions from the homogeneous phases and the interfaces:

$$\Delta_{tot}\phi = \Delta_l\phi + \Delta_{l,a}\phi + \Delta_a\phi + \Delta_{a,e}\phi + \Delta_e\phi + \Delta_{e,c}\phi + \Delta_c\phi + \Delta_{c,r}\phi + \Delta_r\phi \tag{2.21}$$

By assuming that the coefficients λ, r, π, $S^*_{e-,Mo}$ and $S^*_{e-,Pb}$ are temperature independent, the equations for the left side Mo phase are:

$$\Delta_l T = -\frac{d^l}{\lambda^l}\left(J_q'^l - \pi\frac{j}{F}\right) \tag{2.22}$$

$$\Delta_l\phi = -\frac{1}{F}S^*_{e-,Mo}\Delta_l T - r^l d^l j, \tag{2.23}$$

where d^l is the thickness of phase l. Similar expressions as equation (2.22)-(2.23) can be written for the remaining homogeneous phases, as well as for the interfaces. See chapter 14 in [6] for the derivation of these expressions. By inserting all these expressions into equation (2.21), an expression for the total cell potential can be found. All coefficients refer to the stationary state. The electrodes are thermostatted at $T^{s,l} = T^{a,l} = T^{a,e} = T^{s,a} = T^{s,l} \equiv T^a$ and $T^{s,c} = T^{c,e} = T^{c,r} = T^{s,r} \equiv T^c$ and when the electric current density is zero and the temperature dependence of the enthalpy is neglected, equation (2.21) becomes:

$$\Delta_{tot}\phi = \frac{1}{F}[S^*_{e-,Mo} - \frac{1}{2}(S^{*,e}_{Pb^{2+}} - S_{Pb})](T^c - T^a) \tag{2.24}$$

This means that equation (2.15) can be written as

$$\eta_E = \left(\frac{\Delta_{tot}\phi}{\Delta T}\right)_{j=0} = \frac{1}{F}[S^*_{e-,Mo} - \frac{1}{2}(S^{*,e}_{Pb^{2+}} - S_{Pb})], \tag{2.25}$$

where S^*_i is the transported entropy and S_i is the thermodynamic entropy.

In this thesis, no electrodes are present. This means that only the bulk phase is studied. Since the Seebeck coefficient in equation (2.25) takes the electrodes into account, this will not be the correct expression to use in this thesis. To develop an expression for the Seebeck coefficient when no electrodes are present, the entropy production needs to be defined.

By considering an isotropic polarizable medium where a heat flux is present, the entropy production can be written as [10]:

$$\sigma = -\frac{1}{T}\frac{\partial P}{\partial t}(E_{eq} - E) + J_q^{'}\left(\frac{\partial}{\partial T}\frac{1}{T}\right) \tag{2.26}$$

where P is the polarization and E_{eq} is the equilibrium electric field given by E_{eq}=P/($\chi_e\varepsilon_0$). χ_e is the electric susceptibility given by χ_e=ε_r-1, where ε_r is the relative dielectric constant. ε_0 is the vacuum permittivity and E is the electrostatic field.

The Seebeck coefficient can then be defined as the ratio between the electric field, E, and the thermal gradient, ∇T:

$$S_E = \frac{E}{\nabla T} \tag{2.27}$$

The electric field is a field produced from electrically charged objects. In the x-direction, E is given by [10]:

$$E(x) = \frac{1}{\varepsilon_0}\int_0^x \rho(x')dx', \tag{2.28}$$

where ε_0 is the vacuum permittivity and $\rho(x')$ is the charge density.

So the difference between the definition of the Seebeck coefficient in equation (2.15) and (2.27) is that no electrodes are present in equation (2.27). The entropy productions given in equation (2.16) and (2.26) are different. In equation (2.16), the displacement current, $\frac{\partial P}{\partial t}$, is equal to 0. In equation (2.26), the electric potential gradient, $\frac{\partial \phi}{\partial x}$, is 0. This means that the two definitions of the Seebeck coefficient, equation (2.15) and (2.27), are not direct comparable. In equation (2.25), the contribution from the metal phases to the Seebeck coefficient is equal to -$\frac{1}{2}S^{*,e}_{Pb^{2+}}$, so this value may be the closest relation to the values obtain by equation (2.27), since no electrodes are present in equation (2.27).

The electric field can also be analyzed in terms of the monopolar, dipolar and quadrupolar contributions [2]. S. D. Lecce and F. Bresme have shown that the higher order terms can be neglected. M(x) is needed to calculate the monopolar (ionic) contribution to the electric field in the direction of the thermal gradient (x-direction), and is given by:

$$M(x) = \frac{1}{A}\left\langle \sum_{i=1}^{N_{ions}} \delta(x - x_i)q_i \right\rangle, \tag{2.29}$$

where A is the cross sectional area (=$L_y L_z$) of the simulation box, N_{ions} is the number of ions, δ is the delta function, x is the position in the box, x_i is the position of the oxygen atom in the water molecule, q_i is the charge of the ion.

The dipolar contribution to the electric field can be calculated from $P_x(x)$, and $P_x(x)$ is given by:

$$P_x(x) = \frac{1}{A}\left\langle \sum_{i=1}^{N_m} \delta(x - x_i)\left[\sum_{j=1}^{j\in m} q_{j,m} x_{j,m}\right]\right\rangle, \tag{2.30}$$

where N_m is the number of molecules, j is the subindex for the number of charged sites in each molecule, $x_{j,m}$ is the x-coordinate of site j (the hydrogen site) in molecule m in the molecular frame of reference (which means that oxygen is in the center [12]), and $q_{j,m}$ is the charge of site j.

$Q_{xx}(x)$, needed to calculate the quadrupole contribution to the field, is given by [2]:

$$Q_{xx}(x) = \frac{1}{A}\left\langle \sum_{i=1}^{N_m} \delta(x - x_i)\left[\frac{1}{2}\sum_{j=1}^{j\in m} q_{j,m} x_{j,m}^2\right]\right\rangle \tag{2.31}$$

For the pure water system, see section 5.2.1, only the dipolar and quadrupolar terms contribute to the total electric field. For the electrolyte solution, see section 5.2.4, all of the terms presented in equation (2.29)-(2.31) contribute to the total electric field. For the electrolyte solution, the total electric field is given by:

$$\begin{aligned} E(x) &= E_M(x) + E_{P_x}(x) + E_{Q_{xx}}(x) \\ &= \frac{1}{\varepsilon_0}\int_0^x \rho_{q_{ion}}(x')dx' - \frac{1}{\varepsilon_0}\int_0^x \frac{dP_x(x')}{dx'}dx' + \frac{1}{\varepsilon_0}\int_0^x \frac{d^2Q_{xx}(x')}{dx'^2}dx', \end{aligned} \tag{2.32}$$

where $\rho_{q_{ion}}$ is the charge density for the ions.

2.3 The Soret effect

Diffusive mass transport due to a thermal gradient is called the Soret effect [11]. The reciprocal effect of the Soret effect is the Dufor effect, and it is heat transport due to a gradient in concentration. When the heat- and mass transport take place in the x-direction, the entropy production for a two-component system can be written as

$$\sigma = J_q^{'} \frac{\partial}{\partial x}\left(\frac{1}{T}\right) + J_1\left(-\frac{1}{T}\frac{\partial \mu_{1,T}}{\partial x}\right) \tag{2.33}$$

where σ is the entropy production, $J_q^{'}$ is the measurable heat flux, T is the temperature, J_1 is the mass flux of component 1 and $\mu_{1,T}$ is the chemical potential of component 1 at constant temperature. The linear flux-force relation for $J_q^{'}$ can be written as

$$J_q^{'} = L_{qq}\frac{\partial}{\partial x}\left(\frac{1}{T}\right) + L_{q\mu}\left(-\frac{1}{T}\frac{\partial \mu_{1,T}}{\partial x}\right) \tag{2.34}$$

and for J_1 it is expressed as

$$J_1 = L_{\mu q}\frac{\partial}{\partial x}\left(\frac{1}{T}\right) + L_{\mu\mu}\left(-\frac{1}{T}\frac{\partial \mu_{1,T}}{\partial x}\right) \tag{2.35}$$

According to the Onsager relations $L_{q\mu}$=$L_{\mu q}$. The L's describe diffusive transport of heat and mass. When the temperature is constant, equation (2.35) reduces to

$$J_1 = L_{\mu\mu}\left(-\frac{1}{T}\frac{\partial \mu_{1,T}}{\partial x}\right) \tag{2.36}$$

The chemical potential for a non-electrolyte is

$$\mu_1 = \mu_1^{\circ} + \mathrm{RTln}\gamma_1 c_1 \tag{2.37}$$

Equation (2.36) can be related to Fick's law, given in equation (2.6), by

$$J_1 = -L_{\mu\mu}\frac{1}{T}\frac{\partial \mu_{1,T}}{\partial x} = -L_{\mu\mu}\frac{1}{T}\frac{\partial \mu_{1,T}}{\partial c_1}\frac{\partial c_1}{\partial x} = -D_{1,2}\frac{\partial c_1}{\partial x} \tag{2.38}$$

where the interdiffusion coefficient of the first component $D_{1,2}$ is equal to

$$D_{1,2} = \frac{L_{\mu\mu}}{T}\left(\frac{\partial \mu_{1,T}}{\partial c_1}\right) = \frac{L_{\mu\mu}R}{c_1}\left(1 + \frac{\partial \mathrm{ln}\gamma_1}{\partial \mathrm{ln}c_1}\right) \tag{2.39}$$

If the chemical potential of component 1, $\mu_{1,T}$, is constant, then equation (2.34) reduces to Fourier's law for a homogeneous system

$$J_q^{'} = L_{qq}\frac{\partial}{\partial x}\left(\frac{1}{T}\right) = -\lambda_\mu \frac{\partial T}{\partial x} \tag{2.40}$$

The following relation between the thermal conductivity and L_{qq} can be obtained from equation (2.40)

$$\lambda_\mu = -\left(\frac{J_q^{'}}{\partial T/\partial x}\right)_{\partial\mu/\partial x=0} = \frac{1}{T^2}L_{qq} \tag{2.41}$$

When the chemical potential is constant, the mass flux in the solvent frame of reference is given by

$$J_1 = L_{\mu q}\frac{\partial}{\partial x}\left(\frac{1}{T}\right) = -c_1 D_T \frac{\partial T}{\partial x} \tag{2.42}$$

where the thermal diffusion coefficient, D_T, is defined by

$$D_T = \frac{L_{\mu q}}{c_1 T^2} \tag{2.43}$$

When the system is in a stationary state (i.e. J_1=0), the Soret coefficient can be defined as

$$s_T \equiv -\left(\frac{\partial c_1/\partial x}{c_1 \partial T/\partial x}\right)_{J_1=0} = \frac{D_T}{D_{1,2}} \tag{2.44}$$

So the Soret coefficient is equal to the ratio of the concentration and the temperature gradients, at zero mass flux, which is also equal to the ratio of the thermal diffusion coefficient and the interdiffusion coefficient, which is defined in equation (2.43) and (2.39), respectively.

The Soret coefficient can also be defined in terms of mole fractions:

$$s_T = -\frac{1}{x_1 x_2}\frac{dx_1/dx}{dT/dx}, \tag{2.45}$$

where x_1 and x_2 are the mole fractions of component 1 and 2, respectively.

The Soret coefficient is usually negative for the light component and positive for the heavy component in a binary mixture. The heavier component tends to migrate to the cold region, and the lighter component tends to migrate to the hot region. The Soret coefficient is expected

to be higher when there is a large difference in masses between the components, compared to when the difference is smaller. The magnitude of the Soret coefficient is also influenced by the molecular diameter-ratio [13]. If there is a large difference in molecular diameter for the species, a higher Soret coefficient is expected, compared to when the molecular diameter-ratio is equal to 1.

2.4 Electrolyte solutions

Electrolyte solutions are solutions that conduct electrical power [14]. NaCl in water is an example of an electrolyte solution. Here, water is the solvent and NaCl is the solute. When the salt is added to water, NaCl wil dissociate to ions, Na^+ and Cl^-. Because of the ion's ability to transport charges, the electrolyte solution conducts electrical power.

The understanding of Coulmbic interactions is central in electrolyte solutions. Because of the electrostatic interactions, charges of opposite signs attract each other and charges of equal signs repel each other. The absolute value of the Coloumb force between two charged particles is given by:

$$F = \frac{q_1 q_2}{4\pi\varepsilon_0\varepsilon_r r^2}, \tag{2.46}$$

where q_1 and q_2 are the magnitude of the two charges, ε_0 is the vacuum permittivity, ε_r is the relative permittivity and r is the distance between particle 1 and 2.

Strong electrolytes have a higher electrical conductivity compared to week electrolytes. Strong electrolytes ionize completely, while week electrolytes ionize only partially. An example of a strong electrolyte is KCl in water and a week electrolyte is CH_3COOH in water.

The ions in the electrolyte solution can have different ionic mobilities, which means that the ions move with different velocities when the system is exposed to a voltage difference. The ion mobility, μ, is defined as [15]:

$$\mu = \frac{v}{E}, \tag{2.47}$$

where v is the stationary velocity of the ion in a constant electric field and E is the electrical field. The ion mobility depends both on particle size and particle charge. The ion mobility is inversely proportional to the particle diameter, which means that particles with a larger diameter have a lower mobility.

By the Einstein relation, the ion mobility is proportional to the diffusion coefficient, D [16]:

$$\mu = \frac{zDF}{RT}, \tag{2.48}$$

where z is the charge number, F is Faraday's constant, R is the gas constant and T is the temperature. The diffusion coefficient can be related to the molar mass. Particles with high molar mass migrate more slowly, which means they have a lower diffusion coefficient. Since the ion mobility is proportional to the diffusion coefficient, this means that particles with a higher molar mass have a lower mobility compared to particles with a lower molar mass.

2.5 Dipole and quadrupole moment

An electric dipole consists of two electric charges +Q and -Q separated by a distance R [16]. The magnitude of the dipole moment is given by

$$\mu = QR, \tag{2.49}$$

where Q is the charge, and R is the distance between the charges. When a molecule has a permanent electric dipole, it is called a polar molecule. A permanent dipole moment stems from nonuniform distributions of the charge density through the molecule. The magnitude of the dipole moment can also be calculated from the dipole vectors in the x-, y-, and z-directions:

$$\mu = \sqrt{\mu_x^2 + \mu_y^2 + \mu_z^2}, \tag{2.50}$$

where μ_x is given by

$$\mu_x = \sum_i Q_i x_i \tag{2.51}$$

Q_i is the partial charge of atom i and x_i is the x-coordinate of atom i.

The quadrupole moment, **q**, has 9 components [16]:

$$\mathbf{q} = \begin{pmatrix} q_{xx} & q_{xy} & q_{xz} \\ q_{yx} & q_{yy} & q_{yz} \\ q_{zx} & q_{zy} & q_{zz} \end{pmatrix}, \tag{2.52}$$

where q_{xx} is given by

$$q_{xx} = \sum_i Q_i x_i^2 \tag{2.53}$$

3 Computational background

In the following sections, some computational background is presented.

3.1 Molecular Dynamics

Molecular dynamics (MD) is a computer simulation method for generating trajectories that describe how dynamic variables in the system change with time [17]. The configuration of the particles in the system is generated by integrating Newton's equations of motion:

$$m_i \frac{d^2\mathbf{r}_i}{dt^2} = \mathbf{f}_i, \tag{3.1}$$

where m_i is the mass of particle i, $\mathbf{r}_i$ is its position, $\mathbf{f}_i$ is the force acting on it, and t is the time.

MD is a technique for computing the equilibrium and transport properties of a classical many-body system [18]. This means that the nuclear motion of the particles obey the laws of classical mechanics. When the quantity of interest is computed in a MD simulation, the quantity must be expressed as a function of position and momenta of the particles in the system.

3.2 The Verlet algorithm

The Verlet algorithm is an algorithm for integrating Newton's equations of motion [18]. To derive the Verlet algorithm, a Taylor expansion of the coordinate of a particle, around time t, is needed:

$$\mathbf{r}(t+\Delta t) = \mathbf{r}(t) + \mathbf{v}(t)\Delta t + \frac{\mathbf{f}(t)}{2m}\Delta t^2 + \frac{\Delta t^3}{3!}\dddot{\mathbf{r}} + O(\Delta t^4) \tag{3.2}$$

$\mathbf{r}$ denotes the position of the i-th particle, $\mathbf{v}$ denotes its velocity, $\mathbf{f}$ denotes the force it is subjected to, and $\dddot{\mathbf{r}}$ is the third derivative of $\mathbf{r}$ with respect to time. Similarly,

$$\mathbf{r}(t-\Delta t) = \mathbf{r}(t) - \mathbf{v}(t)\Delta t + \frac{\mathbf{f}(t)}{2m}\Delta t^2 - \frac{\Delta t^3}{3!}\dddot{\mathbf{r}} + O(\Delta t^4) \tag{3.3}$$

By summing equation (3.2) and (3.3), the result is:

$$\mathbf{r}(t+\Delta t) + \mathbf{r}(t-\Delta t) = 2\mathbf{r}(t) + \frac{\mathbf{f}(t)}{m}\Delta t^2 + O(\Delta t^4) \tag{3.4}$$

or

$$\mathbf{r}(t+\Delta t) \approx 2\mathbf{r}(t) - \mathbf{r}(t-\Delta t) + \frac{\mathbf{f}(t)}{m}\Delta t^2 \tag{3.5}$$

The estimate of the new position contains an error that is of order Δt^4, and Δt is the time step in the MD simulation. The expression for the velocity is given by

$$\mathbf{v}(t) = \frac{\mathbf{r}(t+\Delta t) - \mathbf{r}(t-\Delta t)}{2\Delta t} + O(\Delta t^2) \tag{3.6}$$

3.3 The Lennard-Jones and Coulomb potentials

In order to model the interactions between the ions, between the water molecules and between the ions and water, the Lennard-Jones and Coulomb potential are used. The potential is given by [18]:

$$V = 4\varepsilon\left(\left(\frac{\sigma}{r}\right)^{12} - \left(\frac{\sigma}{r}\right)^{6}\right) + \frac{q_i q_j}{\varepsilon_0 r}, \tag{3.7}$$

where the first term is the Lennard-Jones potential and it consists of a repulsive and a dispersion term. The second term in equation (3.7) is the Coulomb potential. ε is the depth of the potential well, σ is the distance between the two particles at which the Lennard Jones potential is equal to zero, r is the distance between particle i and j, q_i and q_j are the charges of particle i and j, respectively, and ε_0 is the vacuum permittivity. The parameters in the potential in equation (3.7) are presented in table 3.2 and A.1.

3.4 The SPC/E water model

When water is modelled in a MD simulation, a water model is needed to describe the water structure. In this thesis, the extended simple point charge (SPC/E) water model is chosen. The SPC/E model is a reparametrization of the simple point charge (SPC) model [19]. The SPC/E model has three point masses and the HOH angle is equal to the tetrahedral angle of 109.47°. In this model, the water molecule has rigid bonds. This means that both the OH bonds and the HOH angle are fixed.

The repulsion and dispersion forces in the water molecule are represented by the Lennard-Jones potential and the electrostatic interactions are represented by Coulomb's law, as given

in equation (3.7). The properties of the SPC/E water model are given in table 3.1 [19]:

Table 3.1: Some properties of the SPC/E model: the mass and charge of oxygen and hydrogen, the HOH angle and the bond length of the OH bond.

O mass [g mol^{-1}]	H mass [g mol^{-1}]	O charge	H charge	θ of HOH angle [°]	r$_{OH}$ [Å]
15.9994	1.008	-0.8476	0.4238	109.47	1.0

The Lennard-Jones parameters, ε and σ, for water are given table 3.2. The parameters are needed to describe the equation for the potential, given in equation (3.7).

Table 3.2: The Lennard-Jones parameters, ε and σ, for water. The parameters are needed in equation (3.7).

Interaction	ε [kcal mol^{-1}]	σ [Å]
O-O	0.1553	3.166
O-H	0	0
H-H	0	0

For the Lennard Jones interactions, there are no intra- or intermolecular interactions between oxygen and hydrogen or hydrogen and hydrogen in this water model. There are intermolecular interactions between the oxygens.

3.5 The Ewald summation

The interactions that decay no faster than r^{-n}, where n is the dimensionality of the system, can cause a problem during the simulation [17]. This is because the range of these interactions is often greater than L/2, where L is the box length. The Ewald summation is a method for computing long-range contributions to the potential energy in a system with periodic boundary conditions [18]. This technique reduces the cost of the computations of the long range Coulombic interactions. The Coulombic energy due to all pairs of charges in a simulation box with periodic boundary conditions is given by [17]:

$$V = \frac{1}{2} \sum_{\mathbf{n}} \sum_{i=1}^{N} \sum_{j=1}^{N} \frac{q_i q_j}{4\pi\varepsilon_0 |\mathbf{r}_{ij} + \mathbf{n}|}, \tag{3.8}$$

where **n** is the cubic lattice points, **n** = (n_xL, n_yL, n_zL) with n_x, n_y, n_z being integers and $\mathbf{r}_{ij}$ is the minimum distance between charges i and j. N is the number of charges and i and j are indices. The position of the central box and each image box (due to periodic boundary conditions) can be related by specifying the vectors **i**, **j**, and **k**. The position of each image box is an multiple of the length of the box, ($\pm$**i**L, $\pm$**j**L, $\pm$**k**L).

The problem with equation (3.8) is that the sum converges slowly and conditionally. By using the Ewald summation, the Coulombic interaction energy converges rapidly, but also absolutely. The trick is to convert the summation in equation (3.8) into two series by using the mathematical expression

$$\frac{1}{r} = \frac{f(r)}{r} + \frac{1 - f(r)}{r} \tag{3.9}$$

In the Ewald sum, the complementary error function, erfc(r), is used as f(r). The final expression for the Coulombic potential by using the Ewald summation method becomes [17]:

$$V = \frac{1}{2} \sum_{i=1}^{N} \sum_{j=1}^{N} \begin{cases} \sum_{|\mathbf{n}|=0}^{\infty}{}' \frac{q_i q_j}{4\pi\varepsilon_0} \frac{\mathrm{erfc}(\alpha|\mathbf{r}_{ij}+\mathbf{n}|)}{|\mathbf{r}_{ij}+\mathbf{n}|} \\ + \sum_{k \neq 0} \frac{1}{\pi L^3} \frac{q_i q_j}{4\pi\varepsilon_0} \frac{4\pi^2}{k^2} \exp\left(-\frac{k^2}{4\alpha^2}\right) \cos(\mathbf{k} \cdot \mathbf{r}_{ij}) \\ - \frac{\alpha}{\sqrt{\pi}} \sum_{k=1}^{N} \frac{q_k^2}{4\pi\varepsilon_0} + \frac{2\pi}{3L^3} \Big| \sum_{k=1}^{N} \frac{q_k}{4\pi\varepsilon_0} r_k \Big|^2 \end{cases} \tag{3.10}$$

where the first term is the real space part, the second term is the Fourier part, the third term is the self-interaction part, and the last term is the correction term of the Coulombic potential. The correction term is only included when the surrounding medium is a vacuum.

3.6 Periodic boundary conditions

By using periodic boundary conditions during a computer simulation, a relatively small number of particles can be used because the system is replicated in every direction [17]. This means that particles can interact across a boundary. If particles exit one end of the simulation box, they will reenter the box at the other end. The modelled system is placed in a unit cell, and this unit cell is replicated an infinite number of times.

3.7 Self diffusion coefficient

Movement of particles in a liquid due to the particles' kinetic energy is called Brownian motions [14]. The diffusion due to the Brownian motions is called self diffusion.

There are two different methods for calculating the self diffusion coefficient from a MD simulation [17]. The first method is to calculate the coefficient from the mean square displacement (MSD) according to the formula:

$$D = \lim_{t\to\infty} \frac{\langle|\mathbf{r}(t) - \mathbf{r}(0)|^2\rangle}{2dt}, \tag{3.11}$$

where $\langle|\mathbf{r}(t) - \mathbf{r}(0)|^2\rangle$ is the mean square displacement, d is the dimensionality of the simulation box and t is the time. The angled brackets indicate an ensemble average, which means an average over both all particles and all time origins. Plotting the MSD versus the time should yield a line with a slope proportional to the diffusion coefficient with a proportionality constant equal to 1/2d. The positions used to calculate the MSD can not have had periodic boundary conditions applied to them.

The second approach for calculating the diffusion coefficient is via the velocity auto correlation function (VACF). This is a Green-Kubo integral with the VACF as the argument:

$$D = \frac{1}{d}\int_0^\infty dt\mathbf{v}(t)\mathbf{v}(0)\rangle \tag{3.12}$$

The first approach, finding D by using the MSD, will be used in this thesis. This is because the long-time tail of the VACF converges slowly [20].

3.8 Heat flux and thermal conductivity

There are two ways for computing the heat flux in a MD simulation. The first approach is to compute the flux by the following formula [21]:

$$\boldsymbol{J_q} = \frac{1}{V}\left[\sum_i e_i \mathbf{v}_i - \sum_i \mathbf{S}_i \mathbf{v}_i\right], \tag{3.13}$$

In this thesis, the heat flux is computed in each layer, which means that V is the volume of the layer, e_i is the per-atom energy (potential and kinetic) in each layer, $\mathbf{S}_i$ is the per-atom stress tensor in each layer, and $\mathbf{v}_i$ is the the velocity of particle i in each layer. $\boldsymbol{J_q}$ in equation (3.13) is the total heat flux. In this thesis, the mass flux is zero, which means that the total heat flux is equal to the measurable heat flux. The measurable heat flux of one component, $J_q^{'}$, is given by [6]:

$$J_q^{'} = J_q + H_m J_m, \tag{3.14}$$

where H_m is the partial molar enthalpy of the component and J_m is the mass flux. As mentioned, the measurable heat flux is equal to the total heat flux in this thesis, since the mass flux is equal to zero.

The total heat flux is equal to the internal energy flux, which is also equal to the measurable heat flux in this thesis, and this gives a second approach for calculating the heat flux. The heat flux can be computed by calculating how much energy that is subtracted or added to the cold and hot regions when a thermal gradient is induced. When the thermal gradient is applied in the x-direction, the heat flux can be calculated according to [10]:

$$\boldsymbol{J_q} = \left\{\frac{\pm\Delta u}{2\delta t A}, 0, 0\right\}, \tag{3.15}$$

where $\pm\Delta$u is the energy added (+) or subtracted (-) from the hot or cold regions, δt is the time step and A is the cross-sectional area of the simulation box. In equation (3.15), it is assumed that the heat flux is constant between the hot and cold regions.

The thermal conductivity can be calculated from the Green-Kubo formula [21]:

$$\lambda = \frac{V}{3k_B T^2}\int_0^\infty \langle \mathbf{J}_q(0)\mathbf{J}_q(t)\rangle dt, \tag{3.16}$$

where k_B is Boltzmann's constant and $\langle \mathbf{J}_q(0)\mathbf{J}_q(t)\rangle dt$ is the ensemble average of the auto correlation function of the heat flux.

The thermal conductivity can also be computed from Fourier's law, when the heat flux and the thermal gradient are known [6]:

$$J_q = -\lambda \frac{dT}{dx} \tag{3.17}$$

In this thesis, equation (3.15) will be used for calculating the heat flux, and equation (3.17) will be used for the calculation of the thermal conductivity.

3.9 Thermostatting

The temperature gradient was created by constructing one hot region at each end of the simulation box and one cold region in the middle of the box. The volume of the hot and cold regions are equal, and the simulation box is symmetric around the middle of the box. See figure 4.1 for an illustration of the simulation box, where the hot and cold regions are included. In the hot and cold regions, the velocities of the atoms were rescaled every 10th time step in order to tend to the target temperatures. The velocities were only rescaled if the temperature deviated 0.0001 K or more from the target temperature.

3.10 Ensembles

In this thesis, the canonical (NVT), the isothermal-isobaric (NPT) and the microcanonical (NVE) ensembles are used.

The canonical ensemble is used during the equilibriation of the different systems, as stated in section 4. In the NVT ensemble, the number of particles, the volume, and the temperature are fixed [18]. For controlling the temperature in the NVT ensemble, the Nosé Hoover thermostat is used. In the Nosé Hoover thermostat, a fictitious dynamic variable is introduced, which is the friction, ζ. The temperature is set to a desired value, and the friction slows down or accelerates the particles until this temperature is reached. The temperature is not fixed when a Nosé-Hoover thermostat is used, but the temperature tends, over time, to the desired target temperature.

In the NPT ensemble, both a Nosé Hoover thermostat and barostat are used. This means that the number of particles, the pressure, and the temperature are kept fixed during the

simulation. In the Nosé Hoover barostat, some dynamic variables, which are coupled to the simulation domain dimensions, are added [18]. In this thesis, the NPT ensemble is used during the equilibriation to obtain the desired liquid density, as described in section 4. In LAMMPS, the equations of motion in the NVT and NPT simulations are those of Shinoda et al. [22]. For time integration, the integrators derived by Tuckerman et al. [23] are used.

In the NVE ensemble, the number of particles, the volume, and the energy are fixed [18]. In this ensemble, Newton's equations of motion are solved without any pressure or temperature control.

4 Methodology

In this thesis, molecular dynamics simulations were performed with the software LAMMPS [24]. The version of 11 August 2017 was used. The trajectories were integrated using the velocity Verlet algorithm described in section 3.2.

The first step in the simulation was to create a suitable start configuration. For water, a molecule file was created. This file contained information needed to define the geometry of water, such as the coordinates of the two hydrogens and the oxygen, the charges of the atoms, and information about the bonds and angles in the molecule. The molecule file created in LAMMPS is given in appendix I.1.

The SPC/E model was used to model water, and the properties of this model are given in table 3.1 and 3.2. The bonds between oxygen and hydrogen and the H-O-H angle were kept fixed with the fix SHAKE command. The Lennard-Jones and Coulomb potential were used to model the interactions, and the parameters are given in table 3.2 for water and in table A.1 for the electrolyte solution consisting of LiCl and water.

The boundary conditions were periodic in the x-, y- and z-directions, which means that the particles can interact across a boundary, as stated in section 3.6. The x-direction was 3 times longer than the y- and z-directions for the pure water system and the electrolyte solution, simulation number 1 and 2 in table 4.1, respectively. This is because the transport in the x-direction was of interest. For system number 3 in table 4.1, the x-direction was 4 times longer than the y- and z-directions. The time step in simulation number 2 and 3 in table 4.1 was equal to 1.0 fs and the time step in simulation number 1 was equal to 2 fs. The cutoff for the Lennard-Jones interaction and the real part of the Ewald sum was set to 10 Å in all systems. The accuracy in the reciprocal space was set to $1{\cdot}10^{-5}$ and tail corrections were included.

For the electrolyte solution, the water structure was defined using the same molecule file as used for modelling the pure water system. The ions were placed randomly in the simulation box. The average salt concentration was equal to 1.01 mol kg^{-1}. How the salt concentration was calculated is shown in appendix E. The next step for both the water system and the electrolyte solution was to perform an NPT simulation in order to obtain the suitable liquid density. For water, this density corresponded to 0.772 g cm^{-3} and the density of the electrolyte solution was equal to 0.99 g cm^{-3}. The equilibration in the NPT ensemble was 1 ns in both systems. An example script for the NPT simulation is given in appendix I.2. For simulation number 3 in table 4.1, LiCl where the dielectric constant for water was used, the desired density was obtained by using a suitable value for the lattice constant. The equi-

libriation was done in the NVT ensemble for this system. The LAMMPS input script is presented in appendix I.4.

For the electrolyte solution and the pure water system, the next step was to do an additional equilibriation in the NVT ensemble (1 ns). During the NPT simulations, the simulation box was cubic. The box was replicated during the NVT simulation, to create a simulation box that was 3 times longer in the x-direction compared to the y- and z-directions. The equilibriation in the NPT and NVT ensemble was performed at an average temperature, T_{ave} = (T_H+T_C)/2, where T_H and T_C corresponds to the hot and cold temperatures in the thermostatted regions during the non-equilibrium simulations. An example script for the NVT simulation is presented in section I.3. After the equilibriation, the temperature gradient was introduced. This was done by creating one hot region at each end of the simulation box and a cold region in the middle of the box. The volume of the hot regions was equal to the volume of the cold region. The simulation box was symmetric around the middle of the box. A description of the thermostatting is given in section 3.9. The particles between the hot and cold regions were assigned the NVE ensemble.

In the hot and cold regions, the velocities of the atoms were rescaled every 10th time step in order to tend to the target temperatures. After the stationary state was reached, the temperature profile, composition profile and pressure profile were computed. Both in the pure water system and in the electrolyte solution, only the water molecules in the hot and cold regions were thermostatted at the target temperatures. Over time, the temperatures of the Li^+ and Cl^- ions in a region will tend to the same value as the temperature of the water molecules in the same region. A note on the degrees of freedom in the temperature calculation is given in appendix D. An example script for the non-equilibrium simulation is presented in appendix I.5.

An illustration of the simulation box including the thermostatted regions is presented in figure 4.1. The box has one hot layer at each end of the box and two cold layers in the middle of the box. The box is symmetric around the middle of the box, as shown in figure 4.1.

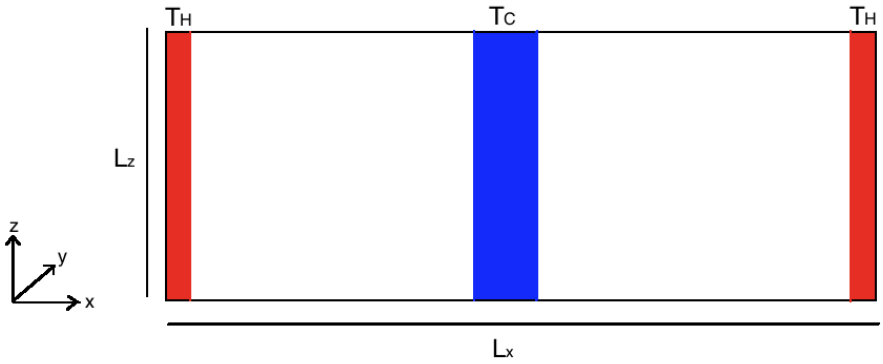

Figure 4.1: An illustration of the simulation box. Periodic boundary conditions were chosen. The box has a hot region at each end of the box and a cold region in the middle of the box. The box is symmetric around the middle.

The different systems constructed in this thesis are presented in table 4.1. The systems constructed are a pure water system, simulation number 1 in table 4.1, an electrolyte solution consisting of LiCl and water, simulation number 2, and a system with LiCl where the dielectric constant for water is used rather than actual water molecules, simulation number 3.

Table 4.1: An overview of the different systems which are created in this thesis. The number of ion pairs, N_{LiCl}, the number of water molecules, N_{H_2O}, the salt concentration, c, the density, ρ, the hot and the cold temperatures, T_H and T_C, and the box dimensions are given for each system.

Simulation no.	System	N_{LiCl}	N_{H_2O}	c [mol kg^{-1}]	ρ [g cm^{-3}]	T_H [K]	T_C [K]	Box dimensions [Å]
1	H_2O	-	3600	-	0.772	600	500	[107.862, 35.954, 35.954]
2	LiCl + H_2O	30	1650	1.01	0.99	450	290	[77.64,25.88,25.88]
3	LiCl with ε_0 for water	520	-	1.01	0.04237	450	290	[240, 60 60]

A snapshot of the electrolyte solution is presented in figure 4.2. The oxygen atoms are red, the hydrogens are grey, the lithiums are green, and the chloride ions are blue.

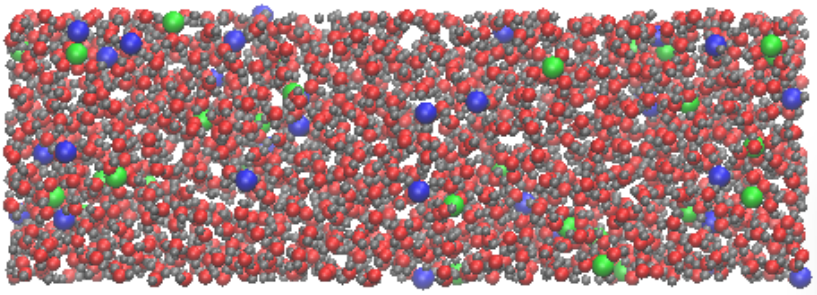

Figure 4.2: A snapshot of the electrolyte solution. The oxygen atoms are red, the hydrogens are grey, the lithiums are green, and the chloride ions are blue.

5 Results and discussion

In the following sections, the results are presented and discussed. Both equilibrium and non-equilibrium MD simulations are performed. In addition, a short discussion on how well the chosen water model reproduces the behaviour of real water is included.

5.1 Equilibrium MD simulations

The next sections include a presentation and discussion of the equilibrium MD simulations performed in this thesis. This includes the self diffusion coefficient of water in simulation number 1 in table 4.1 and the self diffusion coefficients of lithium, chloride and water in simulation number 2 presented in table 4.1.

5.1.1 Self diffusion coefficient for the pure water system

The self diffusion coefficient for pure water was calculated according to equation (3.11), and the plot of the mean square displacement against time is presented in figure 5.1:

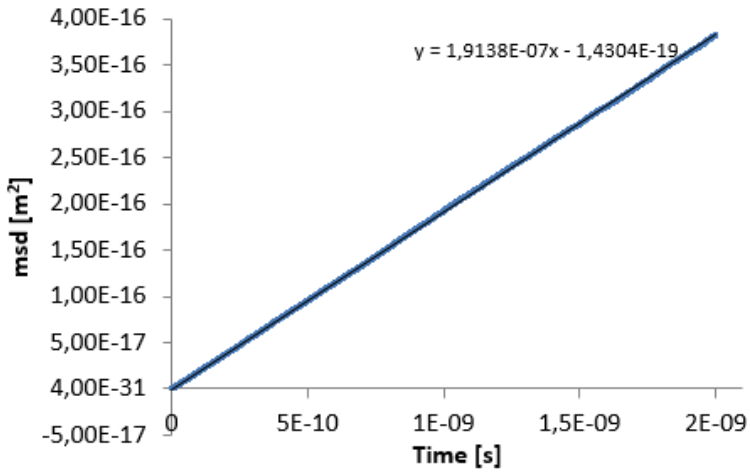

Figure 5.1: A plot of the mean square displacement against time for H_2O.

The slope of the line in figure 5.1 times the proportionality constant equal to 1/6 yields the self diffusion coefficient of water. The coefficient is presented in table 5.1, along with the self diffusion coefficient of water at 550 K obtained with MD simulations by S. H. Lee [3]. The average diffusion coefficient given in table 5.1 was computed from 10 ns. An average profile was computed every 2 ns, and these individual profiles were used to calculate the standard deviation of the mean self diffusion coefficient according to equation (B.1). An

example script for how the self diffusion coefficient was calculated in LAMMPS is presented in appendix I.6.

Table 5.1: The self diffusion coefficient for H_2O at an average temperature of 550 K. The coefficient computed in this thesis is compared to the result obtained by S. H. Lee [3] (marked with an asterisk, *). S. H. Lee also used a temperature of 550 K and the SPC/E water model.

	D·10^8 [m^2 s^{-1}]	D·10^8 [m^2 s^{-1}] (*)
H_2O	3.19 $\pm$0.04	3.01 $\pm$0.03

The diffusion coefficient of water computed in this thesis and the coefficient obtained by S. H. Lee are in good agreement. The self diffusion coefficient obtained in the pure water system is higher compared to the self diffusion coefficient for water obtained in the electrolyte solution, given in table 5.2. This is expected, since the temperature was higher in the pure water system compared to the temperature in the electrolyte solution [4].

5.1.2 Self diffusion coefficients for the electrolyte solution

The self diffusion coefficients for Li^+, Cl^- and H_2O were calculated according to equation (3.11). The calculation of the coefficients were performed in equilibrium. The mean square displacements were calculated for the components and plotted against time. According to equation (3.11), the slope of the line will then be proportional to the self diffusion coefficient with a proportionality constant equal to 1/6.

The plots of the mean square displacement against time for Li^+, Cl^- and H_2O are presented in figure 5.2-5.4, respectively.

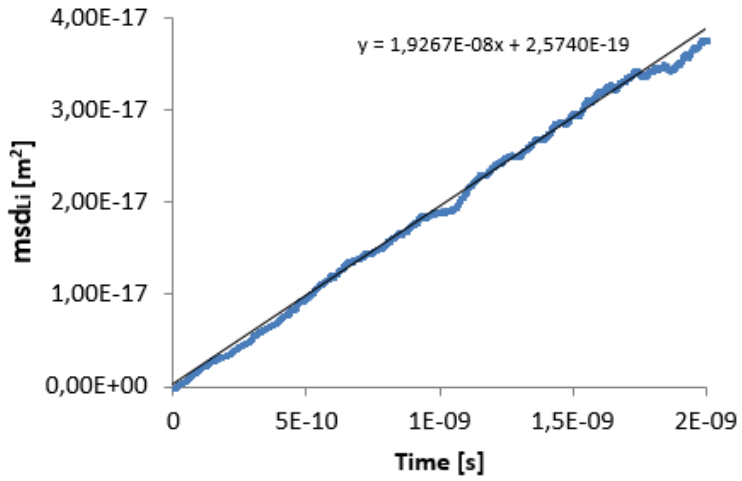

Figure 5.2: A plot of the mean square displacement against time for Li^+.

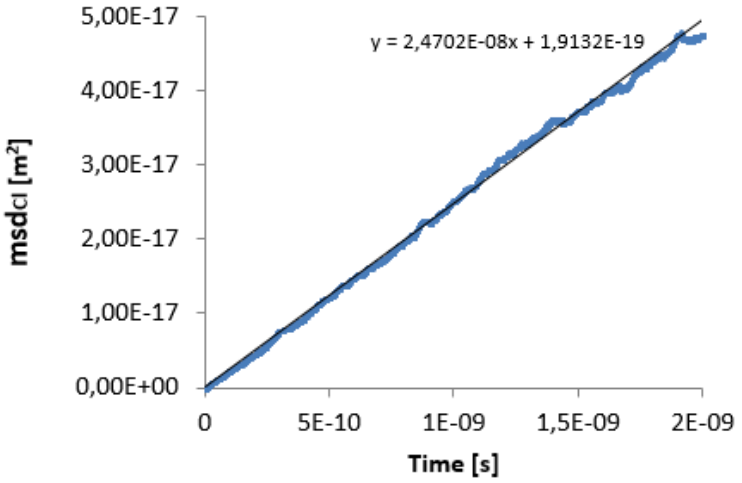

Figure 5.3: A plot of the mean square displacement against time for Cl^-.

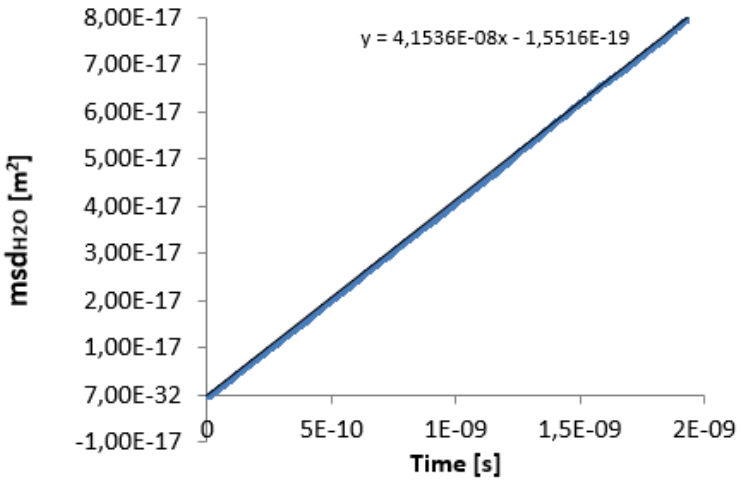

Figure 5.4: A plot of the mean square displacement against time for H_2O.

In figure 5.2 and 5.3 there are some fluctuations, but this is due to the low average salt concentration. By multiplying the slopes of the lines in figure 5.2-5.4 by 1/6, the self diffusion coefficients can be calculated. The coefficients are presented in table 5.2:

Table 5.2: The self diffusion coefficients for Li^+, Cl^- and H_2O with c=1.01 mol kg^{-1} and T=370 K.

	$D \cdot 10^9$ [m^2 s^{-1}]
Li^+	3.2 $\pm$0.2
Cl^-	4.1 $\pm$0.2
H_2O	6.92 $\pm$0.07

The mean square displacements in figure 5.2-5.4 represent an average of 10 ns. An average profile was computed over 2 ns, and this was repeated five times. The five independent profiles were used to calculate the standard deviation of the mean self diffusion coefficient for all the components, according to equation (B.1).

Egorov et al. calculated the self diffusion coefficients of Li^+ and H_2O using MD simulations and the SPC/E water model with an average salt concentration of 1.7 mol kg^{-1} [4]. They have presented the temperature dependence of the self diffusion coefficients of Li^+ and H_2O in figure 11(ii) and 10, respectively, in [4]. By reading from the plots in figure 11(ii) and 10 in [4], the approximate self diffusion coefficients of Li^+ and H_2O at T=370 K are presented in table 5.3:

Table 5.3: The approximate self diffusion coefficients for Li^+ and H_2O with c=1.7 mol kg^{-1} and T is approximately equal to 370 K, computed by Egorov et al. [4]. They have presented the temperature dependence of the self diffusion coefficients of Li^+ and H_2O in figure 11(ii) and 10, respectively, in [4]. The coefficients and the temperature are read off from plots, that is why the coefficients are presented as approximate values in the table.

	D·10^9 [m^2 s^{-1}]
Li^+	~ 2
H_2O	~ 5.9

The self diffusion coefficients presented in table 5.3 are lower compared to the results presented in table 5.2. Egorov et al. also investigated the concentration dependence of the self diffusion coefficients in the electrolyte solution at room temperature. They found that the self diffusion coefficients decrease with increasing salt concentration. Since Egorov et al. used a higher salt concentration than the concentration used in this thesis, 1.7 mol kg^{-1} compared to 1.01 mol kg^{-1}, the self diffusion coefficient should be lower in the result presented by Egorov et al., see table 5.3. This is the case, as observed in table 5.2 and 5.3. Egorov et al. also compared the self diffusion coefficients for Li^+ and H_2O obtained by MD simulations with available experimental results. They found that the self diffusion coefficients of Li^+ and H_2O were slightly lower in MD simulations using the SPC/E water model compared to the coefficients obtained experimentally. This was the result for all temperatures they investigated, which was the range $\sim 260 - 400$K.

As observed in table 5.2 and 5.3, lithium has the lowest diffusion coefficient, which means that this ion has the slowest migration. This means that lithium uses the longest time to reach the stationary state in concentration. The time to reach stationary state can be roughly estimated according to $\tau \sim L^2/D$ [2], where D is the self diffusion coefficient and L is the distance between the hot and the cold regions. For Li^+, the time to reach stationary is approximately equal to 3.5 ns. In comparison, the time to reach stationary state for water is approximately 1.9 ns.

Because hydration shells form around Li^+, this is the component with the lowest self diffusion coefficient. Hydration occurs because water is polar due to its unequal charge distribution on the oxygen and hydrogens [25]. The positive ends of water will attach to the anions and the negative ends will attach to the cations. Because the lithium ion is small, the charge density (charge per volume) is large. Since the water molecules are polar, they will be strongly attached to the small Li^+ ion. This will lead to a slower migration of the lithium ions, which means a lower diffusion coefficient.

Egorov et al. did not present the self diffusion coefficient of chloride, but the trend in the self coefficient of lithium, chloride and water is as expected. Kumar et al. calculated self diffusion coefficients of $1.091 \cdot 10^{-9}$, $1.47 \cdot 10^{-9}$ and $2.32 \cdot 10^{-9}$ m^2 s^{-1} for Li^+, Cl^- and H_2O, respectively, with T=298 K and an average salt concentration of 0.52 mol kg^{-1} [26]. Kumar et. al performed MD simulations using the SPC/E water model. This illustrates the expected trend in the three coefficients; Lithium has the slowest migration because of the hydration shells and water has the fastest migration. The self diffusion coefficients are expected to increase with increasing temperature so it is expected that the coefficients obtained by Kumar et al. are lower.

5.2 Non-equilibrium MD simulations

In the following sections, the non-equilibrium MD simulations are presented and discussed. This includes the electric field and the ratio between the electric field and the temperature gradient in the pure water system, and the Soret coefficient and the Seebeck coefficient for the electrolyte solution. In addition, the electric field was calculated for the system with LiCl where the dielectric constant for water was used, simulation number 3 in table 4.1. The heat flux and the thermal conductivity were also computed for the pure water system and the electrolyte solution.

5.2.1 The electric field and thermopolarization coefficient for the pure water system

A pure water system was constructed in order to study the orientation of the water molecules under a thermal gradient. The system corresponds to simulation number 1 in table 4.1. Bresme et al. discovered that there is an orientation of the water molecules when a thermal gradient is applied, thus leading to an electrostatic field [10].

In this section and in section 5.2.4, the goal was to reproduce the results of Armstrong and Bresme [1], and Lecce and Bresme [2], respectively. The reason for doing this was because it was useful to have done the calculations for the pure water system and the electrolyte solution before the new system consisting of only LiCl was investigated (section 5.2.6), in order to get control of the method. It also gives a better understanding of the results, if the calculations for these two systems are performed before the new system is constructed. If the results of this thesis are in accordance with the results of Armstrong and Bresme, and Lecce and Bresme, it also strengthens their results.

When the temperature gradient was introduced, the temperature in the hot regions was set to

600 K and the temperature in the cold region was set to 500 K. These temperatures are within the liquid region of the phase diagram for the SPC/E water model, see the phase diagram in section H. The system consisted of 3600 water molecules, and water was modelled using the SPC/E water model described in section 3.4. A production run of 50 ns was used in this system, and the time step was set to 2 fs. 10 ns intervals were used in order to calculate the standard deviation of the mean, given in equation (B.1).

The temperature profile for the stationary state is given in figure 5.5. The simulation box was divided into 50 bins. A bin is a volume element in the box with a thickness dx. Each of the hot bins at the ends, see figure 4.1, had a thickness of $\frac{2}{50}L_x$, where L_x is the length of the simulation box in the x-direction, given in table 4.1. The cold region in the middle of the box had a thickness of $\frac{4}{50}L_x$.

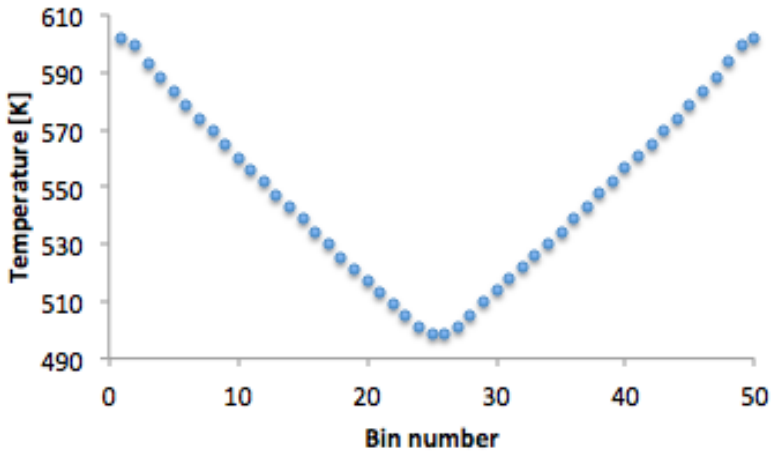

Figure 5.5: The temperature profile for the pure water system. The plot shows the temperature in Kelvin vs. the bin number. The temperature in the hot regions was set to 600 K and the temperature in the cold region was set to 500 K. The hot regions at each end of the box had a thickness of $\frac{2}{50}L_x$, where L_x is the length of the simulation box in the x-direction. The thickness of the cold region in the middle was equal to $\frac{4}{50}L_x$.

The average pressure in the simulation box was approximately equal to 490 atm. The pressure profile is given in figure 5.6. The pressure displayed in figure 5.6 is the P_{xx} component of the pressure tensor, since the direction of the heat flux (x-direction) was of interest.

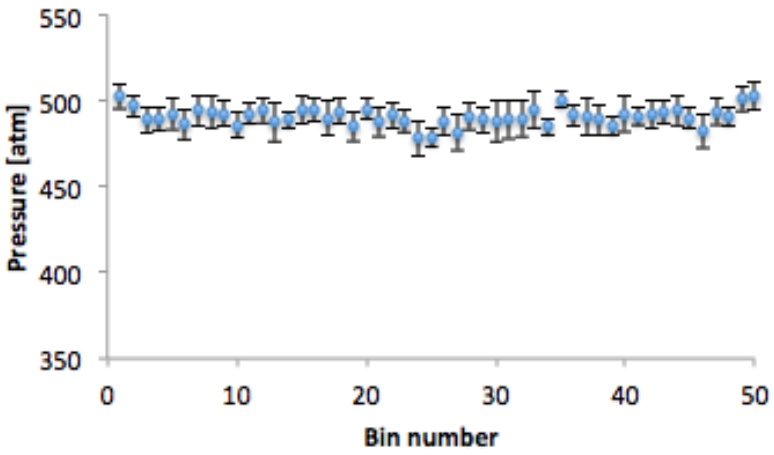

Figure 5.6: The pressure profile for the pure water system. The plot shows the pressure in atm vs. the bin number. The simulation box was divided into 50 bins. The pressure in this figure is the P_{xx} component of the pressure tensor.

J. Armstrong and F. Bresme investigated the pressure and temperature dependence of the ratio between the electric field and the thermal gradient in pure water [1]. As displayed in figure 4 in [1], the ratio between the electric field and the temperature gradient is expected to be large at a temperature of 550 K and at an average pressure of 490 atm, so this was the reason for choosing these conditions in this thesis. It is desirable to avoid the conditions at which the effect is zero. This is because the signal to noise ratio is small when the effect is close to zero, thus making it difficult to extract the real effect. In addition, I. Iriarte-Carretero et al. found that the electric field of water increases with the thermal expansion [27]. The thermal expansion increases dramatically near the critical point.

As presented in section 2.2, the electric field can be calculated by summing the dipolar and quadrupolar contributions to the field. $P_x(x)$ was calculated from equation (2.30) and is presented in figure 5.7:

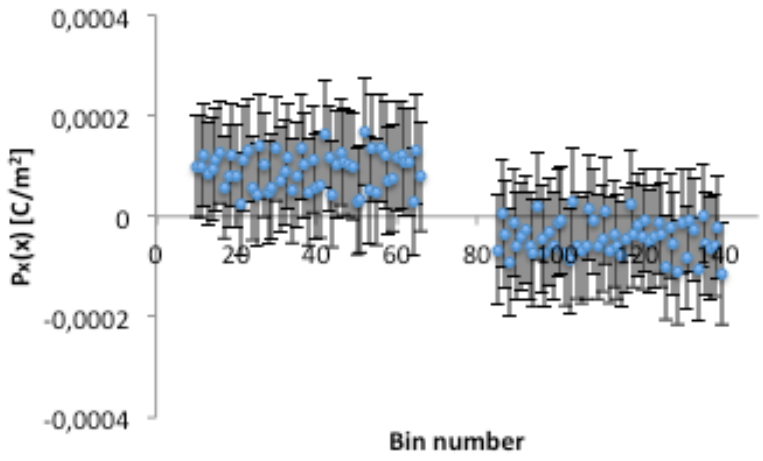

Figure 5.7: $P_x(x)$ plotted against bin number. The whole simulation box is displayed. The standard deviation of $P_x(x)$ is given in the plot, with $\pm 1\sigma$. The simulation box was divided into 150 bins, and 9 bins were neglected at the hot and cold sides of the simulation box, as the thermostat can affect the result.

$Q_{xx}(x)$, calculated from equation (2.31), is presented in figure 5.8:

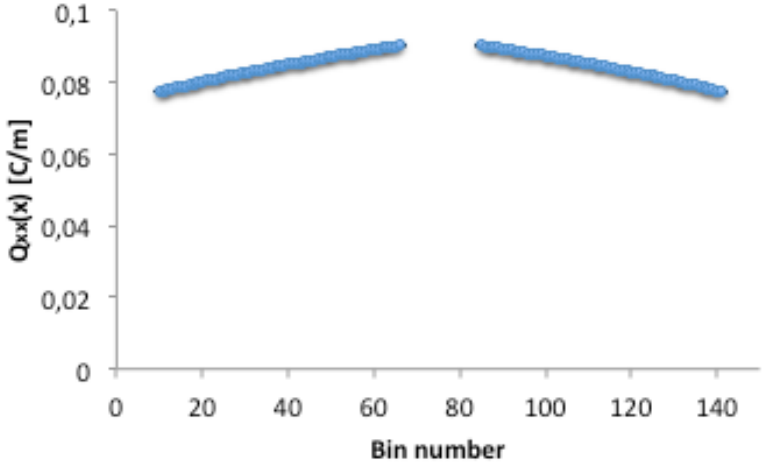

Figure 5.8: $Q_{xx}(x)$ plotted against bin number. The standard deviation of $Q_{xx}(x)$ is shown in the plot, but they are smaller than the points. The simulation box was divided into 150 bins, and the whole box is shown in the plot. 9 bins were neglected at the hot and cold sides of the simulation box.

In figure 5.7 and 5.8, the whole simulation box is displayed. The simulation box was divided into 150 bins, which yielded a bin thickness of approximately 0.7 Å. Armstrong and Bresme used a bin thickness of 0.7 Å [1], so the same thickness was chosen in this thesis in order to have as similar conditions as possible. $P_x(x)$ should be symmetric around the middle of the box, i.e. the same magnitude but opposite sign. Within the statistical error, $P_x(x)$ is

symmetric around the middle of the box. The derivative of $Q_{xx}(x)$ should be symmetric around the middle, see equation (2.32). The standard deviation is given in both figure 5.7 and 5.8, but the errors are smaller than the points in figure 5.8. $P_x(x)$ and $Q_{xx}(x)$ were calculated in a post processing code written in Fortran 95 [28] by Bjørn Hafskjold, and the code is presented in appendix J.3.

$\mathrm{E}_{P_x}(x)$ and $\mathrm{E}_{Q_{xx}}(x)$ were calculated according to equation (2.32) by fitting a line to $P_x(x)$ and fitting a second order polynomial to $Q_{xx}(x)$. One line was fitted to the left hand side and one was fitted to the right hand side in figures 5.7 and 5.8, and the average magnitude of the left and right hand sides was used. To calculate $\mathrm{E}_{P_x}(x)$, the derivative of $P_x(x)$ should be integrated, which is the same as inserting the boundary conditions of the integral into the fitted line for $P_x(x)$. $\mathrm{E}_{Q_{xx}}(x)$ can be calculated by integrating the second derivative of $Q_{xx}(x)$, which is the same as inserting the boundary conditions of the integral into the derivative of the second order polynomial fitted to $Q_{xx}(x)$. The resulting contributions to the field and the total field are given in table 5.4. The strength of the thermopolarization effect can be quantified through the thermopolarization coefficient, $\mathrm{S_{TP}}=\mathrm{E}/\nabla\mathrm{T}$ [1]. The resulting thermopolarization coefficient is also given in table 5.4:

Table 5.4: The dipolar, $\mathrm{E}_{P_x}(x)$, and quadrupolar contributions, $\mathrm{E}_{Q_{xx}}(x)$, to the electric field, and the total electric field for water, $\mathrm{E}_{water}(x)$. The thermopolarization coefficient is also given in the table. The standard deviations of the fields and the coefficient are given in the table.

Contribution	$\mathrm{E}\cdot 10^{-7}$ [V m^{-1}]	$\mathrm{S_{TP}}\cdot 10^{4}$ [V K^{-1}]
$\mathrm{E}_{P_x}(x)$	-0.67 $\pm$0.05	
$\mathrm{E}_{Q_{xx}}(x)$	1.77 $\pm$0.04	
$\mathrm{E}_{water}(x)$	1.10 $\pm$0.05	-5.4 $\pm$0.3

Armstrong and Bresme have calculated the dipolar and quadrupolar contributions to the electric field along with the thermopolarization coefficient for a pure water system at different temperatures and pressures [1]. In figure 3 in [1], they show the dipolar and quadrupolar contributions to the electric field when the average temperature is equal to 550 K ($\mathrm{T_H}$=600 K and $\mathrm{T_C}$=500 K). However, even though the same hot and cold temperatures are used, the system size is different from the size used in this section, which means that the thermal gradient differs from this thesis. Armstrong and Bresme used a cubic box with lengths 39.27 Å [1]. This means that the thermal gradient is larger in the system described by Armstrong and Bresme compared to the gradient in this thesis. This also means that the electric field is expected to be larger in the results obtained by Armstrong and Bresme. This is the case: the dipolar contribution to the electric field calculated in this thesis is equal to (-0.67$\pm$0.05)$\cdot 10^7$

V m^{-1}, while Armstrong and Bresme calculated a contribution approximately equal to -$3{\cdot}10^7$ V m^{-1}. The quadrupolar contribution is equal to $(1.77{\pm}0.04){\cdot}10^7$ V m^{-1} in this thesis, while Armstrong and Bresme obtained a contribution approximately equal to $(9.7{\pm}0.2){\cdot}10^7$ V m^{-1}. A discussion of the sign of the dipolar contribution to the field is presented in section 5.2.2. The results presented by Armstrong and Bresme were obtained at a pressure approximately equal to 300 bar, and the pressure used in this thesis was 490 atm. It can be observed in figure 4 in [1] that the thermopolarization coefficient depends on the pressure.

Armstrong and Bresme computed the thermopolarization coefficient in the range 250-750 K and at pressures 50, 350, 900 and 1500 bar, given in figure 4 in [1]. From this figure, the expected thermopolarization coefficient for the system presented in this thesis with T=550 K and P = 490 atm is approximately -$5.5{\cdot}10^{-4}$ V K^{-1}. The thermopolarization coefficient computed in this thesis is equal to $(-5.4{\pm}0.3){\pm}10^{-4}$ V K^{-1}, which means that the coefficient is in good agreement with the results obtained by Armstrong and Bresme.

The electric field was also calculated from the integral of the charge density, given in equation (2.28). The electric field along with the thermopolarization coefficient are given in table 5.5:

Table 5.5: The electric field calculated from the integral of the charge density, given in equation (2.28), and the thermopolarization coefficient. The standard deviations of the field and the coefficient are given in the table.

$E{\cdot}10^{-7}$ [V m^{-1}]	$S_{TP}{\cdot}10^4$ [V K^{-1}]
1.1 $\pm$0.7	-6 $\pm$3

The electric field plotted against the x position is presented in figure 5.9. In the calculation of the electric field, the simulation box was divided into 150 bins. In figure 5.9, half of the simulation box is included. Since the electric field is expected to be symmetric around the middle of the box, the average magnitude of the symmetric bins was used. 9 bins were neglected at the hot and cold sides of the box. In figure 5.9, cumulative integration is performed in Python 3.6.4 [29], and an example code is presented in appendix J.1.

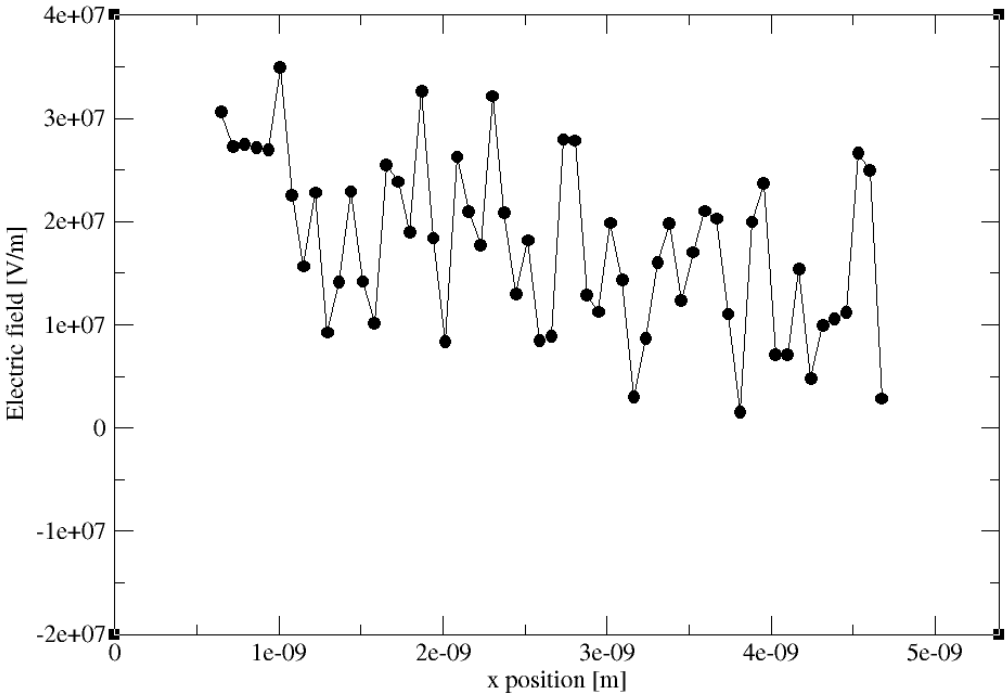

Figure 5.9: The electric field plotted against the x position for the pure water system. The simulation box was divided into 150 bins and half of the box is displayed. The average magnitude of the symmetric bins was used. 9 bins were neglected at the hot and cold sides of the box.

Armstrong and Bresme showed that the electric field calculated from the integral of the charge density, equation (2.28), and the field calculated from the dipolar and quadrupolar contributions, equation (2.32), give the same result [1]. This is also the result in this thesis, as displayed in table 5.4 and 5.5. The electric field for water and the thermopolarization coefficient are equal within the statistical error for the two methods, i.e. when the field is calculated from the dipolar and quadrupolar contributions and when the field is calculated by integrating the charge density.

When the electric field was calculated from the two different methods, the simulation box was divided into 150 bins, as stated above. The bin thickness was chosen to be approximately 0.7 Å in order to use as similar conditions as possible compared to Armstrong and Bresme. However, it is not expected that the field is dependent on how many bins the simulation box is divided into. The choice of number of bins may impact the standard deviation of the field. The simulation box was divided into 50, 150 and 300 bins in order to verify that the number of bins does not affect the value for the electric field. The cumulative integration of the charge density when the box was divided into 50, 150 and 300 bins is presented in figure 5.10. The charge density, i.e. the integrand in equation (2.28), for the three different choices

of bin numbers is also presented in the figure.

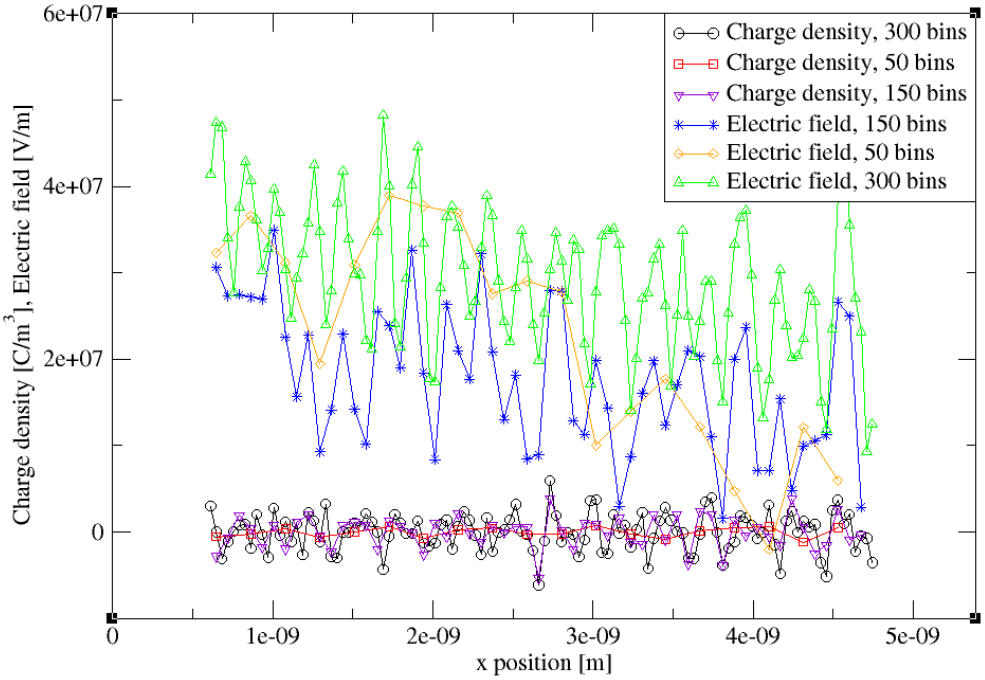

Figure 5.10: The electric field and the charge density vs. the x position for the pure water system. The simulation box was divided into 50, 150, and 300 bins to investigate if the number of bins influences the value for the electric field. The charge density when the box was divided into 300 bins is represented by circles, the charge density when the box was divided into 150 bins is represented by triangles pointing downwards, and the charge density when the box was divided into 50 bins is represented by squares. The electric field for 300 bins is represented by triangles pointing upwards, the electric field for 150 bins is represented by asterisks, and the electric field for 50 bins is represented by diamonds.

The charge densities in figure 5.10 have the expected trend: The charge density has the largest fluctuation when the box is divided into 300 bins and it has the smallest fluctuation when the box is divided into 50 bins. The electric field for the three different number of bins behave differently, but in a cumulative integration, the last point is equal to the total value of the integral. The total integral of the charge density for the three different number of bins are presented in table 5.6:

Table 5.6: The electric field calculated from the integral of the charge density, given in equation (2.28). The standard deviations of the field and the coefficient are given in the table. The simulation box was divided into 50, 150 and 300 bins.

Number of bins	E [V m^{-1}]	S_{TP} [V K^{-1}]
50	(8±7)·10^{6}	(-4±3)·10^{-4}
150	(1.1±0.7)·10^{7}	(-6±3)·10^{-4}
300	(2.1±0.8)·10^{7}	(-1.0±0.4)·10^{-3}

Both the electric field and the thermopolarization coefficient for the three different number of bins are equal within the statistical error, which is the expected result.

5.2.2 Molecular orientation and the sign of $E_{P_{xx}}$

$E_{P_{xx}}$, given in table 5.4, has a negative sign. Since the positive direction of the dipole moment is defined from negative to positive [30], i.e. from oxygen to hydrogen, this means that the dipole moment points towards the hot region. The plan was to study the molecular orientation by computing the cosine to the angle between the dipole vector and the direction of the heat flux (x-direction), cos($\theta_{\mu x}$), vs. the x position. How cos($\theta_{\mu x}$) can be calculated is described in appendix C. The positions of the atoms and the x-, y- and z-components of the dipole vector were stored every 100th time step, and then the average cos($\theta_{\mu x}$) in each bin was calculated with a post processing code in Python 3.6.4 [29]. The code is presented in appendix J.2. However, the value of cos($\theta_{\mu x}$) in each bin is expected to be small, which makes it difficult to extract the real effect. If cos($\theta_{\mu x}$) is plotted against the x-position, and cos($\theta_{\mu x}$)=-1, it means that the dipole vector is parallel to the x-direction, and that the dipole vector points in the opposite direction of the x-axis. J. A. Armstrong and F. Bresme calculated the cosine to the angle between the dipole vector and the direction of the heat flux using the SPC/E water model [30]. They used the Wolf method instead of the Ewald method to handle the electrostatic interactions. However, J. Armstrong, C. D. Daub and F. Bresme discovered 1 year later that how the electrostatic interactions are treated influences the magnitude of the electrostatic field of water [31]. They concluded that the Wolf method overestimates the magnitude of the electrostatic field for water. This means that the cos($\theta_{\mu x}$) also will be overestimated using the Wolf method for handling the electrostatic interactions.

J. A. Armstrong and F. Bresme calculated the cos($\theta_{\mu x}$) as a function of the x position in the box when the thermal gradient was equal to 3.56 K $Å^{-1}$ [30]. The minimum of cos($\theta_{\mu x}$) vs. the x-position between the hot and cold thermostat in figure 5 in [30] is equal to -0.01.

This means that the dipole vector is not parallel to the direction of the heat flux, but it points slightly towards the hot thermostat. Since the Wolf method overestimates the electrostatic field, it means that the minimum value of $\cos(\theta_{\mu x})$ also is overestimated. This means that a small number of $\cos(\theta_{\mu x})$ vs. x position is expected when the Ewald method is used. As stated above, the plan was to calculate $\cos(\theta_{\mu x})$ in this thesis, but since the signal to noise ratio is small, it was difficult to observe the real signal. The expected result of $\cos(\theta_{\mu x})$ as a function of the x-direction is that the cosine values are negative between x=0 and x=L_x/2, since the hot thermostat is at x=0 and the cold thermostat is in the middle of the box. This is because the molecular dipole should point towards the hot side of the box. The reason that the molecular dipole is expected to point towards the hot side is because when a molecule has a mass asymmetry, then the heavier end, oxygen, favours to point towards the cold side. The lighter end, hydrogen, favours to point towards the hot side of the box. This is analogous with the Soret effect in binary mixtures [32]. From the sign of $E_{P_{xx}}$, it can be concluded that the molecular dipole has the expected direction, i.e. pointing towards the hot side of the box.

5.2.3 The heat flux and thermal conductivity for the pure water system

The heat flux and the thermal conductivity were calculated from equation (3.15) and (3.17), respectively. The resulting heat flux and thermal conductivity are given in table 5.7:

Table 5.7: The heat flux and thermal conductivity for the pure water system.

J_q [W m^{-2}]	λ [W m^{-1} K^{-1}]
$(1.320\pm0.002)\cdot10^{10}$	0.676 ± 0.001

The average heat flux and thermal conductivity were calculated over 12 ns. F. Römer et al. calculated the temperature dependence of the thermal conductivity at a density equal to 0.8 g cm^{-1} [33]. The density in the system described in this section was equal to 0.772 g cm^{-3}. It can be observed from figure 4 in [33] that Römer et al. calculated a thermal conductivity equal to 0.67$\pm$0.04 W m^{-1} K^{-1} at T=624 K and ρ=0.8 g cm^{-3}. The average temperature was 550 K in the system investigated in this thesis, and the thermal conductivity is expected to decrease with decreasing temperature [33]. Within the statistical error, the results are in good agreement.

5.2.4 The Soret and Seebeck coefficient for the electrolyte solution

An electrolyte solution consisting of LiCl and water was constructed in order to investigate the Seebeck effect and the Soret effect. The results in this thesis are compared to the results obtained by Lecce and Bresme, given in [2]. In the system presented in this section, a production run of 85 ns was used. An average profile was calculated over 5 ns, and this was repeated 17 times. The 17 independent profiles were used in the calculation of the standard deviation of the mean, given in equation (B.1). Before the production run, the first 15 ns was neglected to ensure that the composition was in the stationary state. The temperature profile reached the stationary state after less than 1 ns.

Lecce and Bresme investigated the Soret effect and the Seebeck effect in the following aqueous alkali haldie solutions: LiCl, KCl, NaCl, NaI, and NaF [2]. At 335 K, Lecce and Bresme found the largest Seebeck coefficient in the electrolyte consisting of LiCl and water. This was the reason for choosing the aqueous LiCl system in this master's thesis, because it is convenient to choose a system where the effect is expected to be large, in order to have a large signal to noise ratio. The coefficient is expected to be of the magnitude 10^{-4} V K^{-1} at 335 K, which is a large effect compared to i.e. aqueous NaF, which is of the order 10^{-3} V K^{-1} at the same conditions [2]. The Soret coefficient is also expected to be large at the chosen conditions in this section.

The temperature profile for the system at stationary state is given in figure 5.11. The figure shows temperature plotted against bin number, and the box was divided into 30 bins. This system corresponds to simulation number 2 in table 4.1. There was one hot region at each end of the simulation box, see figure 4.1, and these regions had a thickness of $\frac{1}{30}\mathrm{L}_x$, where L_x is the length of the simulation box in the x-direction, given in table 4.1. The cold region in the middle of the box had a thickness of $\frac{2}{30}\mathrm{L}_x$. The temperature in the hot regions was set to 450 K and the temperature in the cold region was set to 290 K. The temperatures are within the liquid region of the phase diagram. The phase diagram of pure water is presented in appendix H. When salt is added to water, the melting point is lowered and the boiling point increases [14]. The average salt concentration in the simulation box was equal to 1.01 mol kg^{-1}, and the salt concentration was calculated as described in appendix E. The system consisted of 1650 water molecules, 30 lithium ions and 30 chloride ions.

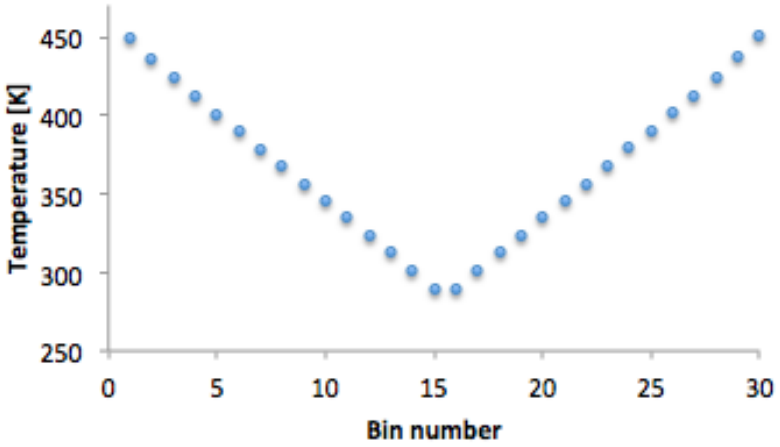

Figure 5.11: The temperature plotted against the bin number for the electrolyte solution. The temperature in the hot regions was set to 450 K and the temperature in the cold region was set to 290 K. There is a hot region at each end of the box, with a thickness $\frac{1}{30}L_x$, and a cold region in the middle with a thickness $\frac{2}{30}L_x$. L_x is the length of the x-direction.

The average pressure in non-equilibrium was equal to 687 atm. The pressure as a function of bin number is presented in figure 5.12. The pressure displayed in figure 5.12 is the P_{xx} component of the pressure tensor, since the direction of the heat flux (x-direction) was of interest.

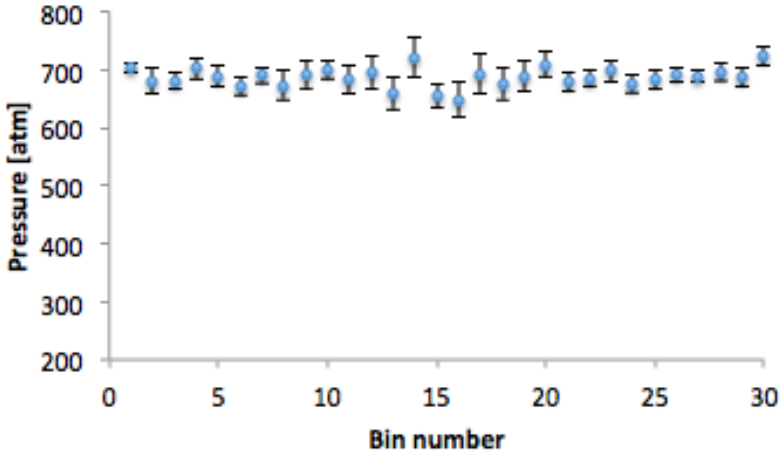

Figure 5.12: The pressure plotted against the bin number for the electrolyte solution. $\pm 2\sigma$ is given in the plot. The simulation box was divided into 30 bins. The pressure in this figure is the P_{xx} component of the pressure tensor.

Lecce and Bresme used a pressure of 600 bar [2]. It was difficult to obtain the exact same pressure in the simulations in this thesis, but 678 atm is close to the value that Lecce and Bresme used.

The mole fraction of LiCl and H_2O vs. the bin number when the thermal gradient was applied is given in figure 5.13 and 5.14, respectively:

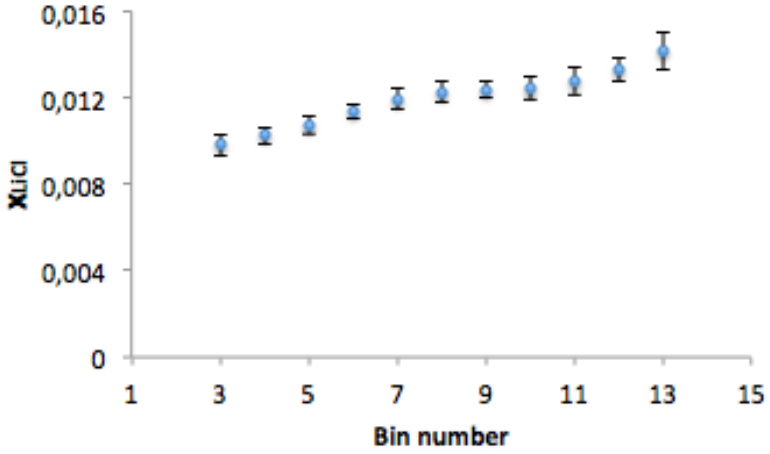

Figure 5.13: The mole fraction of LiCl vs. the bin number and $\pm 2\sigma$ is given in the plot. The symmetric parts of the box were summed and half of the box is displayed. Two bins on the hot and cold sides were neglected since the thermostats can affect the result.

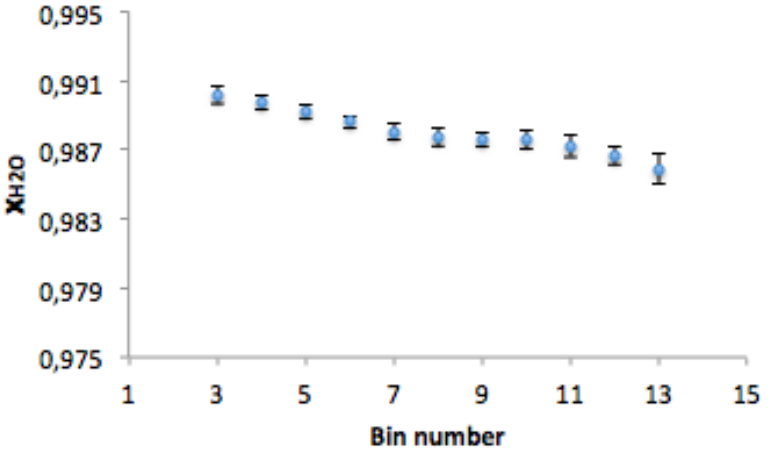

Figure 5.14: The mole fraction of H_2O vs. the bin number. Half of the box is displayed in the plot, and the symmetric parts of the box were summed. Two bins on the hot and cold sides were neglected. $\pm 2\sigma$ is given in the plot.

In figure 5.13 and 5.14, the symmetric bins in the box are summed, i.e. bin 1 and 30, bin 2 and 29, bin 3 and 27, etc. Because the thermostats can affect the results, two bins at the hot and cold sides were neglected from the calculations.

As observed in figure 5.13 and 5.14, there is a mass separation due to the thermal gradient, which means that there is a Soret effect in this system. Figure 5.13 shows that LiCl migrates

to the cold side of the box. Since LiCl is the heavier component compared to water, this is the expected result as presented in section 2.3. From figure 5.14 it can be observed that H_2O, the lighter component, migrates to the hot side of the box. Lithium and chloride are present as ions, not as a molecule, but they will migrate together as a result of the electroneutrality condition.

The Soret coefficient was calculated from equation (2.45), where component 1 was chosen to be LiCl and component 2 was H_2O. $\frac{dx_1/dx}{dT/dx}$ in equation (2.45) was computed by plotting the mole fraction of LiCl vs. the temperature in the box, given in figure 5.15:

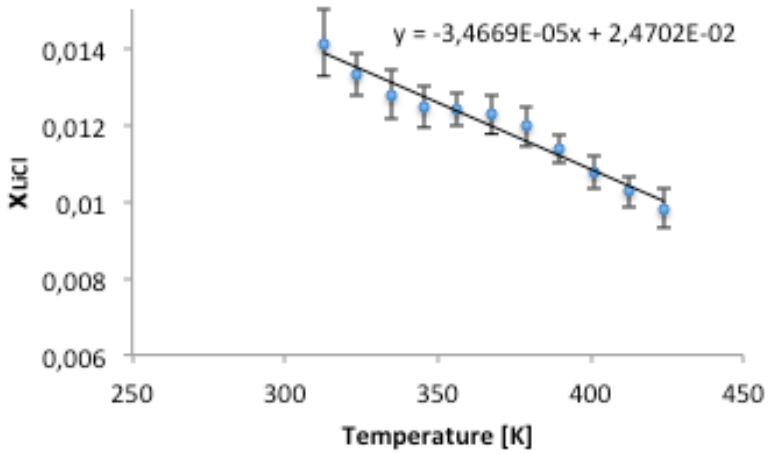

Figure 5.15: The mole fraction of LiCl vs. the temperature. The slope of the line is needed in the calculation of the Soret coefficient.

The slope of the line in figure 5.15 is equal to $\frac{dx_1/dx}{dT/dx}=\frac{dx_1}{dT}$. The resulting Soret coefficient is presented in table 5.8, along with the coefficient calculated by Lecce and Bresme, given in [2]. In table 5.8, the result obtained by Lecce and Bresme is marked with an asterisk, and the value for the coefficient is obtained by reading from figure 2 in [2].

Table 5.8: The Soret coefficient calculated in this thesis and the Soret coefficient calculated by Lecce and Bresme [2]. The coefficient calculated by Lecce and Bresme is marked with an asterisk, *.

$s_T \cdot 10^3$ [K^{-1}]	$s_T \cdot 10^3$ [K^{-1}]$(*)$
3.6 ± 0.4	~ 3.75

The Soret coefficient calculated in this thesis is in good agreement with the coefficient obtained by Lecce and Bresme within the statistical error.

The electric field can be computed from two different methods, by integrating the charge density, equation (2.28), and by summing the mono-, di-, and quadrupolar contributions to the field, equation (2.32). P_x(x) and Q_{xx}(x) are needed for the calculation of the dipolar and the quadrupolar contributions to the electric field, see equation (2.30) and (2.31), respectively. The contributions to the electric field were calculated with a post processing code in Fortran 95 [28]. P_x vs. the bin number is given in figure 5.16:

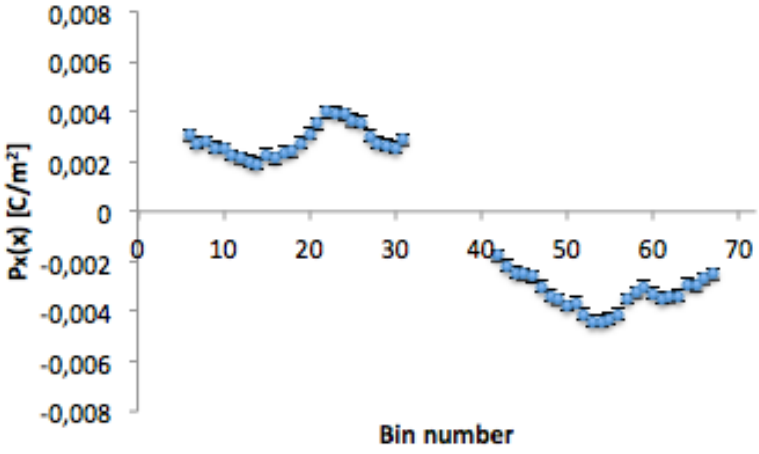

Figure 5.16: P_x vs. the bin number, which is needed to calculate the dipolar contribution to the electric field. The box was divided into 72 bins, and the whole box is shown in the figure. Five bins were neglected at the hot and cold sides. $\pm 1\sigma$ is shown in the plot.

The simulation box was divided into 72 bins, as shown in figure 5.16, and five bins were neglected at the hot and cold sides. The bin thickness was equal to 1.08 Å, and Lecce and Bresme used a bin thickness of 1.07 Å [2]. Q_{xx} is needed in the calculation of the quadrupole contribution to the electric field, and Q_{xx} vs. the bin number is given in figure 5.17:

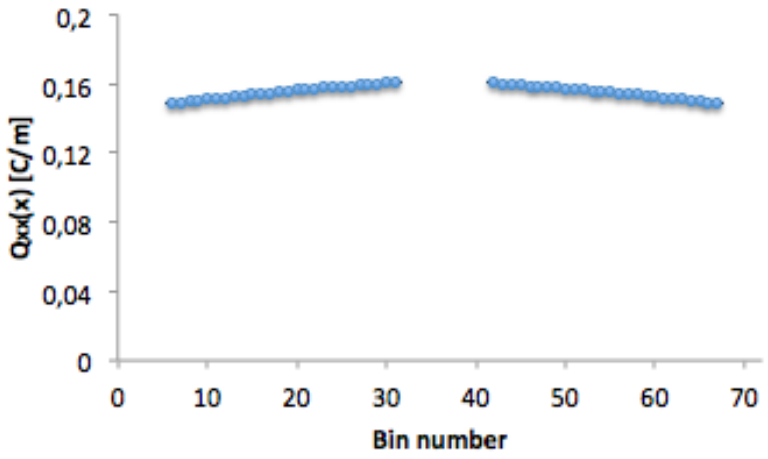

Figure 5.17: Q_{xx} vs. the bin number, which is needed to calculate the quadrupole contribution to the electric field. The whole box is shown in the figure, and $\pm 1\sigma$ is included, but the standard deviation is smaller than the points. The box was divided into 72 bins, and five bins were neglected at the hot and cold sides.

The standard deviations are given in figure 5.16 and 5.17, but the standard deviation is smaller than the points in figure 5.17. To calculate the dipolar and quadrupolar contributions to the field, a straight line was fitted to P_x and a second order polynomial was fitted to Q_{xx}. One line was fitted to the left hand side and one was fitted to the right hand side in figure 5.16 and 5.17, and the average magnitude was used in the calculation of the field. To calculate the dipolar contribution, given in equation (2.32), the derivative of P_x should be integrated, which is the same as inserting the boundary conditions of the integral into P_x. To calculate $E_{Q_{xx}}$ the second derivative of Q_{xx} should be integrated, which is the same as inserting the boundary conditions of the integral into the derivative of Q_{xx}. The monopolar contribution was calculated according to equation (2.29). The resulting mono-, di-, and quadrupole contributions to the field are presented in table 5.9:

Table 5.9: The mono-, di-, and quadrupole contributions to the electric field and the total electric field of the electrolyte solution. The standard deviations of the contributions are given in the table.

Contribution	E·10^{-8} [V m^{-1}]
$E_M(x)$	3 ± 1
$E_{P_x}(x)$	-4.6 ± 0.6
$E_{Q_{xx}}(x)$	0.29 ± 0.05

It can be observed from table 5.9, that the dipolar and quadrupolar contributions to the field

in the electrolyte solution have the same sign as the contribution to the field in the pure water system, presented in section 5.2.1. Since the sign of $E_{P_x}(x)$ is the same as in the pure water system, this means that the oxygen points towards the cold side and hydrogen points towards the hot side, as discussed in section 5.2.2. However, there is an important difference between the dipolar and quadrupolar contributions in the electrolyte solution and in the pure water system. In the pure water system, the quadrupole contribution is larger than the dipole contribution, while in the electrolyte solution, the dipole contribution is larger than the quadrupole contribution. Armstrong and Bresme discovered in a pure water system that the quadrupole contribution increases with increasing temperature [1], so the results obtained in this thesis are in agreement with this. Lecce and Bresme also found that in alkali halide aqueous solutions, the dipole contribution is the dominant term [2], so the results in this thesis agree with this as well.

The contribution from the ions to the electric field is equal to $E_M(x)$, and the contribution from water is equal to $E_{P_x}(x)$+$E_{Q_{xx}}(x)$. The resulting fields from the ions and water are presented in table 5.10, along with the Seebeck coefficient for the electrolyte solution:

Table 5.10: The electric field from the ions and water, along with the total electric field for the electrolyte solution. The Seebeck coefficient is also given in the table. The standard deviation of the contributions and the Seebeck coefficient are given in the table. The electric field was obtained by calculating the mono-, di-, and quadrupole contributions to the field, given in (2.32).

Contribution	$E \cdot 10^{-8}$ [V m^{-1}]	$S_E \cdot 10^{3}$ [V K^{-1}]
E_{ions}	3 $\pm$1	
E_{water}	-4.4 $\pm$0.6	
E_{tot}	-2 $\pm$1	4 $\pm$3

The electric field can also be calculated from the integral of the charge density, given in equation (2.28). The electric field due to the ions and water computed using equation (2.28) is presented in table 5.11:

Table 5.11: The table includes the electric field from ions, water, the total electric field, and the Seebeck coefficient for the electrolyte solution. The standard deviations are also given in the table. The electric field was calculated from the integral of the charge density, given in (2.28).

Contribution	$E \cdot 10^{-8}$ [V m^{-1}]	$S_E \cdot 10^4$ [V K^{-1}]
E_{ions}	6.8 $\pm$0.9	
E_{water}	-6.4 $\pm$0.9	
E_{tot}	0.4 $\pm$0.1	-8 $\pm$3

The cumulative integration of the charge density is shown in figure 5.18. The field contributions from the ions and water are shown, along with the total electric field.

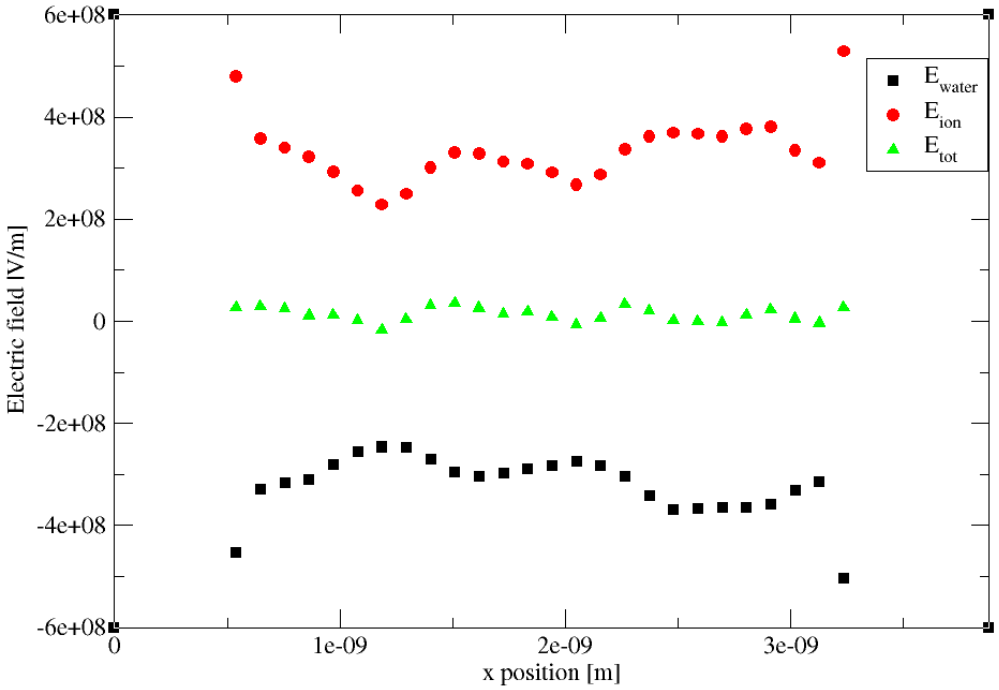

Figure 5.18: The electric field plotted against the x position for the electrolyte solution. The field due to the ions, E_{ion}, the field due to water, E_{water}, and the total field, E_{tot}, are displayed. E_{ion} is represented by circles, E_{water} with squares, and E_{tot} with triangles. The simulation box was divided into 72 bins and half of the box is displayed. The average magnitude of the symmetric bins were used. Five bins were neglected at the hot and cold sides of the box.

Lecce and Bresme showed that using the integral of the charge density, equation (2.28), and summing the mono-, di-, and quadrupole contributions to the electric field, equation (2.32),

should yield the same value for the electric field [2]. This is not the result in this thesis as displayed in table 5.10 and 5.11. Lecce and Bresme obtained a Seebeck coefficient of approximately -1.2·10^{-4} V K^{-1} at an average temperature of 335 K [2]. They did not calculate the coefficient at 370 K, but they did calculate the coefficient in the range 265-335 K. From the trend in the coefficients in the given temperature range, the Seebeck coefficient is expected to be approximately -3·10^{-4} V K^{-1} at 370 K. In this thesis, the Seebeck coefficient obtained from the integral of the charge density is equal to (-8$\pm$3)·10^{-4} V K^{-1} and the coefficient obtained from the mono-, di-, and quadrupole contributions is equal to (4$\pm$3)·10^{-3} V K^{-1}. This means that the coefficient obtained from the integral of the charge density is closest to the value that is expected from the trend in the results by Lecce and Bresme. However, within the statistical errors presented in this thesis, the Seebeck coefficients obtained by the two different methods are neither equal nor in agreement with Lecce and Bresme's results. On the other hand, Lecce and Bresme did not present the standard deviation of the field or the Seebeck coefficient. As observed in table 5.10 and 5.11, the standard deviation of the Seebeck coefficient is of the same order of magnitude as the value of the coefficient. This means that the standard deviation is large, which shows that it is important to include the standard deviation. If Lecce and Bresme had included the standard deviation of the Seebeck coefficient, the coefficient equal to (-8$\pm$3)·10^{-4} V K^{-1} calculated in this thesis may be equal to Lecce and Bresme's results within the statistical error. Since they did not include the standard deviation, it is difficult to say how different the results are.

Lecce and Bresme found that the ion and water contributions to the electric field have opposite signs, and that these contributions are one order of magnitude larger than the total field [2]. In addition, they found that the total field has the same sign as the water contribution at low temperatures (< 305 K for LiCl) and that it has the same sign as the ion contribution at high temperatures (> 305 K for LiCl). Both the contribution from the ions and water need to be considered when the Seebeck coefficient for the electrolyte solution is calculated, otherwise the Seebeck coefficient will be overestimated [2]. In this thesis, when the field was calculated by integrating the charge density, the results are in agreement with the findings of Lecce and Bresme. They also established that the inversion temperature for aqueous LiCl is at approximately 305 K. At the inversion temperature, the Seebeck coefficient is equal to zero, and $S_E > 0$ at T < 305 K and $S_E < 0$ at T > 305 K.

The standard deviations of the field due to the ions and the total electric field presented in table 5.10 are large. The Seebeck coefficient has the opposite sign as predicted by Lecce and Bresme [2]. In table 5.10, the sign of the ion and water contributions are in agreement with table 5.11 and in agreement with the sign that Lecce and Bresme found for the contributions [2]. However, the ion contribution is expected to be larger than the water contribution to

the field. Within the statistical errors of the ion and water contributions, the ion contribution can be larger than the water contribution. Again, this shows the importance of including the standard deviation before a conclusion can be made. However, it is clear from the results obtained in this thesis that it is difficult to get an accurate value for the Seebeck coefficient because of the large variation in both the field and in the coefficient.

In order to reproduce the results obtained by Lecce and Bresme, the intention was to use as similar conditions as possible. However, there are some differences in the methodology and the conditions. Lecce and Bresme performed the simulations in Gromacs, while the simulations in this thesis were performed in LAMMPS. The reason for choosing LAMMPS in this thesis, was because the master student is familiar with this software from the project thesis last semester. In the supplementary material in [2], Lecce and Bresme showed that LAMMPS and Gromacs should yield the same result for the Seebeck coefficient.

The pressure is also slightly different in this system compared to the system investigated by Lecce and Bresme, 678 atm compared to 592 atm [2]. It was difficult to obtain exact the same pressure as they used. The difference in the pressure might have affected the result. Armstrong and Bresme investigated the pressure dependence of the Seebeck coefficient in pure water, given in figure 4 in [1]. It can be observed from figure 4 in [1] that the Seebeck coefficient varies more with the pressure at high temperatures (>500 K) compared to low temperatures (250-400 K). The trend at high temperatures is that the ratio between the electric field and the thermal gradient increases with increasing pressure. It is difficult to say how much the difference in pressure has influenced the result in this system, but since the difference was 86 atm, this might have affected the results. However, the average temperature was equal 370 K, thus the expected outcome is that the pressure difference had less impact on the results when compared to a system a higher average temperature.

The system size is also slightly different from the size that Lecce and Bresme used [2]. In this thesis, the y- and z-directions had a length of 25.88 Å, while Lecce and Bresme used 35.5 Å. The x-direction was 3 times longer than the y- and z-directions. The size of the system may have influenced the result, since a smaller system means a smaller number of atoms, which can lead to poorer statistics compared to a higher number of atoms. Especially, a small system can lead to poor statistics for the contribution from the ions to the field, since the average salt concentration was low. The system size presented in table 4.1 was chosen in this thesis, because the computational cost increases significantly if the y- and z-directions are increased with 10 Å. Since the production run consisted of 85 ns, it was desirable to try to keep the system size small, but still be able to reproduce the results obtained by Lecce and Bresme. It is difficult to say how much the system size influenced the results, but it is likely that the system size has the largest influence on the standard deviation and not on the field

or Seebeck coefficient itself. It can be observed in table 5.10 and 5.11 that the field from the ions has the larger standard deviation compared to water. It would have been useful to use a larger system to get a more accurate value and more reliable results. In the pure water system, section 5.2.1, the two methods for calculation calculating the electric field gave the same value for the electric field, and the calculated thermopolarization coefficients were equal within the statistical error. The results are also in agreement with the results obtained by Armstrong and Bresme [1]. In the pure water system, the system size was larger, which can indicate that a larger system size would have been preferable for the electrolyte solution as well.

This master's thesis have been able to reproduce the Soret coefficient calculated by Lecce and Bresme within the statistical error. However, the Seebeck coefficient is not equal to the one calculated by Lecce and Bresme. It is suspected that the Seebeck effect is a sensitive effect, as discussed above, which makes it more difficult to reproduce this result.

5.2.5 Heat flux and thermal conductivity for the electrolyte solution

The heat flux for the electrolyte solution was calculated according to equation (3.15). In equation (3.15) it is assumed that the heat flux is constant between the hot and cold regions. The heat flux was computed after the stationary state was reached in both temperature and composition. The total heat flux and the measurable heat flux are equal since the mass flux is equal to zero, as explained in section 3.8. The thermal conductivity was calculated from equation (3.17). The resulting heat flux and thermal conductivity are given in table 5.12:

Table 5.12: The heat flux and thermal conductivity for the electrolyte solution.

J_q [W m^{-2}]	λ [W m^{-1} K^{-1}]
$(3.619 \pm 0.005) \cdot 10^{10}$	0.816 ± 0.001

The standard deviation of the mean was calculated according to equation (B.1), and the average was computed from 10 ns.

F. Römer et al. investigated the temperature and density dependence of the thermal conductivity for water using the SPC/E water model [33]. Since the salt concentration in this system was low, 1.01 mol kg^{-1}, it is expected that the thermal conductivity of the electrolyte solution will be close to the value for pure water at the same temperature and density. Since adding salt to water will decrease the thermal conductivity [33], it is expected that the thermal conductivity is slightly lowered compared to the results obtained by F. Römer et al. The average

temperature in the electrolyte solution was equal to 370 K and the density was approximately 1 g cm^{-3}. From figure 4 in [33] it can be observed that F. Römer et al. obtained a thermal conductivity approximately equal to 0.9 W m^{-1} K^{-1} for water at 370 K. Since adding salt to water lowers the thermal conductivity, the result in this thesis is in good agreement with the result obtained by F. Römer et al.

The thermal conductivity calculated for the electrolyte solution at 370 K is higher compared to the thermal conductivity calculated for pure water at 550 K, given in table 5.7. The thermal conductivity is expected to increase with increasing temperature for a given density, but the it is also expected to decrease with decreasing density [33]. The temperature in the pure water system is higher compared to the temperature in the electrolyte solution, but the density is lower for the pure water system. This means that the thermal conductivity is lower for the pure water system compared to the electrolyte solution, and the results are in accordance with the results presented by F. Römer et al. [33].

5.2.6 The electric field for the system with LiCl and dielectric constant for water

A system consisting of LiCl where the dielectric constant for water was used rather than including actual water molecules was constructed in order to investigate if the contribution from the ions to the Seebeck effect in the electrolyte solution depends on the water molecules present in the solution. This corresponds to simulation number 3 in table 4.1. Since it was found in section 5.2.4 that both the ions and the water molecules need to be taken into account in the calculation of the Seebeck coefficient for the electrolyte solution, the expected result was that the contribution from the ions to the Seebeck effect depends on the water molecules.

The simulation box was 4 times longer in the x-direction compared to the y- and z-directions, see table 4.1. The same salt concentration as in the electrolyte solution, simulation number 2 in table 4.1, was used in this case. A description of how the density was calculated is presented in appendix F. The density in the system was equal to 0.04237 g cm^{-3}. The system consisted of 520 lithium ions and 520 chloride ions. The dielectric constant for water is expected to decrease with increasing temperature, and for a temperature equal to 373 K, using the SPC/E water model, M. R. Reddy and M. Berkowitz calculated a dielectric constant of water equal to 51$\pm$0.35 [34]. The temperature in this thesis was equal to 370 K, and a dielectric constant equal to 51 was used. M. R. Reddy and M. Berkowitz used the reaction field method for handling the electrostatic interactions, while the Ewald method was used in this thesis. The value for the dielectric constant seems reasonable and it is not expected that a small change in the constant will have a large impact on the results presented in this section.

Since no water molecules were included, this system is a one-component system. A Soret effect is not expected in a one-component system, but the Seebeck effect can occur. Since the dielectric constant was set to 51, it means that the contribution from the Coulombic interactions become smaller compared to the Coulombic expression when ε_0=1. Changing the value of the dielectric constant from 1 to 51 does not affect the range of the potential.

The hot temperature was set to 450 K and the cold temperature was set to 290 K, the same as in simulation number 2, see section 5.2.4. The temperature profile is given in figure 5.19. The simulation box was divided into 60 bins, and the hot regions at each end of the box had a thickness of $\frac{2}{60}\mathrm{L}_x$, where L_x is the length of the simulation box in the x-direction. The thickness of the cold region in the middle was equal to $\frac{4}{60}\mathrm{L}_x$.

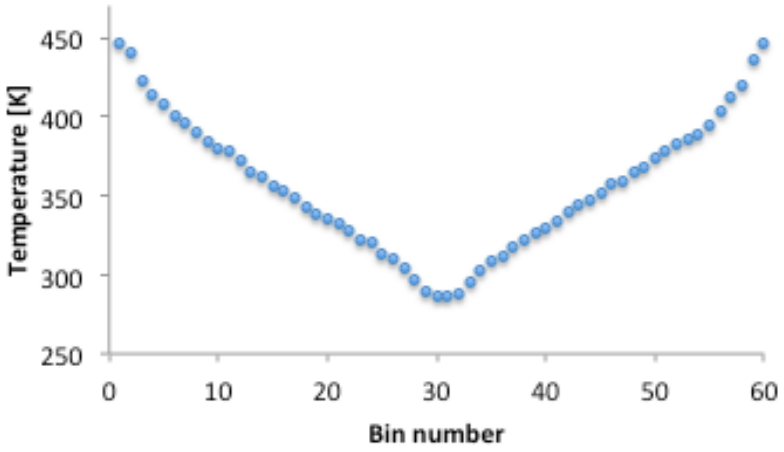

Figure 5.19: The temperature profile for the system consisting of LiCl where the dielectric constant for water was used rather than including water molecules. The temperature is plotted against the bin number. The simulation box was divided into 60 bins, and the hot regions at each end of the box had a thickness of $\frac{2}{60}\mathrm{L}_x$, where L_x is the length of the simulation box in the x-direction. The thickness of the cold region in the middle was equal to $\frac{4}{60}\mathrm{L}_x$.

The temperature profile given in figure 5.19 is not as linear as the temperature profiles given in figure 5.11 and 5.5. This is because the density of LiCl was low. The density of LiCl was the same as in simulation number 2 in table 4.1, but since no water molecules were included, the number of atoms was lower, which lead to poor statistics in the temperature profile.

The average pressure in the x-direction of the simulation box was 47 atm. The pressure profile is given in figure 5.20:

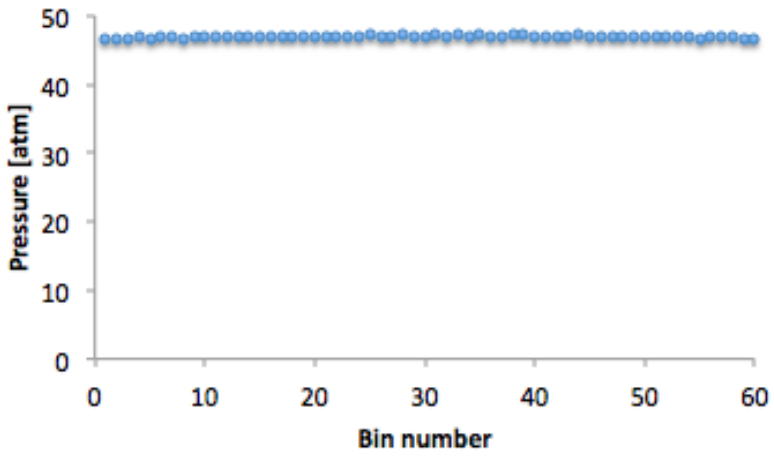

Figure 5.20: The pressure profile for the system with LiCl where the dielectric constant for water was used. The plot shows the pressure in atm vs. the bin number. The standard deviation of the mean pressure is smaller than the points in the plot. The simulation box was divided into 60 bins. The pressure in this figure is the P_{xx} component of the pressure tensor.

After the stationary state was reached, the electric field was calculated. The average electric field was calculated from 8 ns. When the electric field was calculated, the box was divided into 200 bins, and the field was calculated from the integral of the charge density, given in equation (2.28). The electric field vs. the bin number is shown in figure 5.21. Half of the box is shown in the figure. When the field was calculated, the average magnitude of the symmetric parts was used. 8 bins were neglected at the hot and cold sides of the simulation box.

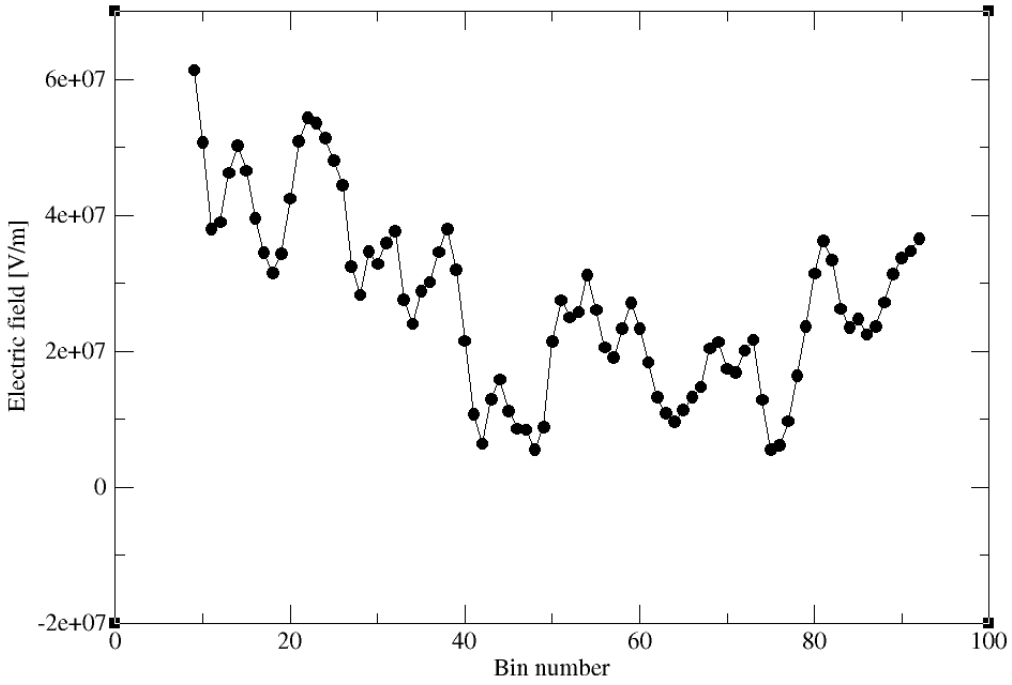

Figure 5.21: The electric field vs. the bin number. The box is divided into 200 bins, and half of the box is displayed in the figure. The average magnitude of the symmetric parts was used. 8 bins were neglected at the hot and cold sides of the box.

Figure 5.21 shows that there is an electric field present in the system consisting of LiCl where the dielectric constant for water was used rather than including actual water molecules. The total electric field along with the Seebeck coefficient is presented in table 5.13:

Table 5.13: The electric field and the Seebeck coefficient for simulation number 3 in table 4.1.

E [V m^{-1}]	S_E [V K^{-1}]
(4±1)·10^7	(-3±1)·10^{-3}

One of the goals of this master's thesis was to investigate if the contribution from the ions to the Seebeck coefficient in the electrolyte solution given in section 5.2.4 depends on the water molecules present in the solution. It is therefore interesting to compare the results presented in table 5.13 with the results given in table 5.11. In the results presented in table 5.11, the electric field was calculated from the integral of the charge density, and the same method was used in this section. The ratio between the electric field and the thermal gradient is equal to (-3±1)·10^{-3} V K^{-1} in the system presented in this section, while the ratio is equal to (-8±3)·10^{-4} V K^{-1} in the electrolyte solution. The coefficients are different within the statistical error, but they have the same sign. It is also interesting to compare the con-

tribution from the ions to the Seebeck coefficient in the electrolyte solution to the Seebeck coefficient computed in this section. By dividing the electric field contribution from the ions presented in table 5.11 by the thermal gradient, the Seebeck coefficient contribution due to the ions is equal to (-1.5$\pm$0.2)$\cdot 10^{-2}$ V K^{-1}. This contribution is one order of magnitude larger compared to the coefficient computed in this section.

It was found in section 5.2.4 that both the ion and water contributions need to be taken into account when the Seebeck coefficient is calculated for the electrolyte solution. This is because the electric fields due to the ions and water have opposite signs, which means that the Seebeck coefficient will be overestimated if only the electric field contribution from the ions is taken into account. From the results obtained in this section it can be concluded that the Seebeck coefficient is different when the water molecules are present compared to when they are not present. This seems reasonable, since the system presented in this section is only a simplified way to model an electrolyte solution, because the water molecules were not included. The interactions between the ions and water were not included, and it is reasonable that they influence the result.

The results presented in this section also indicate that the presence of the water molecules does influence the contribution to the electric field from the ions in an electrolyte solution. However, as discussed in section 5.2.4, the Seebeck effect is a complex effect that may depend on several properties of the system, such as pressure and system size. The average pressure in this system was equal to 47 atm, while the pressure was equal to 687 atm in the electrolyte solution. In addition, the sizes of the systems are different. In other words, additional simulations are needed in order to make a clear conclusion, but the results obtained in this master's thesis indicate that the electric field contribution from the ions to the Seebeck effect in an electrolyte solution depends on the water molecules present in the solution.

It is expected that there is a shielding effect in both the electrolyte solution and in the system presented in this section. This will affect the magnitude of the Coulombic interactions. In the system presented in this section, the magnitude of the Coulombic potential was reduced by 1/51, because a dielectric constant equal to 51 was used. It is expected that the presence of the water molecules in the electrolyte solution leads to a larger shielding effect compared to the system presented in this section. In addition, there is hydration in the electrolyte solution, as stated in section 5.1.2. This means that the positive ends of water will attach to the anions and the negative ends will attach to the cations. This can also lead to additional shielding. Due to the long ranged Coulombic interactions between the ions, the ions leads to an additional shielding effect. Charges of equal sign repel each other and charges of unequal sign attract each other [35]. This leads to a shell formation of alternating charges. Around a given charge, the shell formation acts as a shield. If another charge is at a given distance from the charge in

the centre, the interaction between the two charges are smaller compared to if there were no shell formation. According to Debye Hückel theory, the Coulombic potential will become screened because of the ions [14]. The screening will affect the range of the potential, and the range is determined by the Debye length. The Debye length decreases with increasing concentration of the ions. As stated above, the ion contribution to the Seebeck coefficient in the electrolyte solution is larger than the Seebeck coefficient calculated in this section, and this can be a result of a larger shielding effect in the electrolyte solution, because of the presence of the water molecules.

Since water is one of the most important solvents in biology and materials science [9], it is necessary to get a better understanding of water's response to a thermal gradient. This master's thesis have contributed to a better understanding of this, because it is found that the ion contribution to the Seebeck effect in an electrolyte solution depends on the water molecules. To get an even better understanding of the role of water in the electrolyte solution, a systematic study of the pressure and system size dependence of the Seebeck coefficient for the system presented in this section is suggested. Only one salt concentration was investigated in this thesis. Since this salt concentration was low, 1.01 mol kg^{-1}, it means that there was much more water compared to the number of ions in the system. Therefore, for further studies, it would also be interesting to vary the salt concentration, to investigate if the difference between the Seebeck coefficient calculated in this section and for the electrolyte solution depends on the salt concentration.

5.3 How well does the SPC/E model reproduce the behaviour of real water?

When water is simulated in a MD simulation, a water model is needed in order to describe the water structure. In this thesis, the extended simple point charge model (SPC/E) was chosen to be the water model. In this section, it will be discussed how good the water model reproduces the behaviour of real water.

One important difference between the real water structure and the structure in the SPC/E model, is that the bonds are rigid in the SPC/E model. This means that the O-H bonds and the H-O-H angle are fixed. The H-O-H angle in the model is equal to 109.47 ° [19], and in actual water it is observed to be 104.5 ° [36].

The melting temperature of water in the SPC/E model is equal to 215 K [37] and for real water, the melting point is at 273 K [36]. The critical point in the SPC/E model is 638.6 K [37] and for real water it is 647.096 K [36]. The normal boiling point is 595 K [38] in the SPC/E model and 373 K for real water [36].

The thermal conductivity of water at room temperature is 0.606 W m^{-1} K^{-1} [39], while it is equal to 0.67$\pm$0.04 W m^{-1} K^{-1} [39] at 300 K for the SPC/E model. The self diffusion coefficient of water at room temperature is $2.3 \cdot 10^{-9}$ m s^{-1} [40] and in the SPC/E model the coefficient is equal to $2.54 \cdot 10^{-9}$ m s^{-1} [41]. The dipole moment of real water is 1.85 D [36], and with the SPC/E model it is equal to 2.351 D [19].

The SPC/E model differs from real water in all properties mentioned above. Non of the water models available reproduce water perfectly, but the SPC/E and the TIP4P/2005 are the most accurate models available [41]. Because the SPC/E model is one of the most accurate force fields available for water, it was reasonable to choose this model. In addition, one of the goals of this thesis was to reproduce some of the results obtained by Lecce and Bresme [2], and Armstrong and Bresme [1]. They used the SPC/E model, so it was necessary to choose the same model in order to get results that are comparable.

Even though the SPC/E model is one of the most accurate models available for reproducing real water, it needs to be emphasized that the results obtained in this thesis will be different from real water. However, this model gives an insight into the response of real water to a temperature gradient.

6 Conclusion

Non-equilibrium molecular dynamics simulations were performed in order to investigate the Soret effect and the Seebeck effect in an electrolyte solution consisting of LiCl and water. The results were compared to the results obtained by Lecce and Bresme [2]. The electric field and the thermopolarization coefficient in a pure water system were calculated and compared to results obtained by Armstrong and Bresme [1]. One of the goals was to investigate if the contribution from the ions to the Seebeck effect in an electrolyte solution depends on the water molecules present in the solution. This was investigated by constructing a system consisting of LiCl, where the dielectric constant for water was used rather than including the water molecules, and the electric field and Seebeck coefficient were calculated for this system. The thermal conductivity of the pure water system and the electrolyte solution were also calculated. Additionally, equilibrium molecular dynamics simulations were performed and the self diffusion coefficients for lithium, chloride and water were calculated and compared to values in the literature.

Both the thermal conductivities and the self diffusion coefficients calculated in this thesis were found to be in good agreement with values available in the literature.

In the pure water system and in the electrolyte solution, the electric field was calculated from two methods: by integrating the charge density, equation (2.28), and by summing the mono- (for the electrolyte solution), di- and quadrupole terms to the electric field, equation (2.32). Lecce and Bresme have shown that the two methods should yield the same result for the electric field, and that higher terms than the quadrupole can be neglected [2]. The electric field in the pure water system at an average temperature of 550 K was found to be $(1.10\pm0.05)\cdot10^{7}$ V m^{-1} when the field was calculated from the integral of the charge density, and it was equal to $(1.1\pm0.7)\cdot10^{7}$ V m^{-1} when the dipolar and quadrupolar contributions to the field were summed. The field calculated from the two methods are equal within the statistical error, and in agreement with the results presented by Armstrong and Bresme [1]. The thermopolarization coefficient calculated from the two methods was found to be $(-5.4\pm0.3)\cdot10^{-4}$ V K^{-1} and $(-6\pm3)\cdot10^{-4}$ V K^{-1}, respectively. From the sign of the dipolar contribution to the electric field, it was concluded that the dipole moment of water points towards the hot side of the simulation box.

This master's thesis has been able to reproduce the Soret coefficient for the electrolyte solution computed by Lecce and Bresme. The coefficient calculated in this thesis was equal to $(3.6\pm0.4)\cdot10^{-3}$ K^{-1}, and Lecce and Bresme obtained a coefficient approximately equal to $3.75\cdot10^{-3}$ K^{-1} [2].

The total electric field calculated from equation (2.28) in the electrolyte solution, at an average temperature of 370 K, was equal to $(4\pm1)\cdot10^{7}$ V m^{-1}. The contribution from the ions to the total field was equal to $(6.8\pm0.9)\cdot10^{8}$ V m^{-1} and the contribution from the water molecules was equal to $(-6.4\pm0.9)\cdot10^{8}$ V m^{-1}. This yielded a Seebeck coefficient equal to $(-8\pm3)\cdot10^{-3}$ V K^{-1}. Lecce and Bresme calculated the coefficient in the temperature range 265-335 K [2]. From the trend in the coefficient in this range, the expected Seebeck coefficient is estimated to be $-3\cdot10^{-3}$ V K^{-1} at 370 K. Lecce and Bresme did not give the standard deviation of the coefficients or the fields, so it is difficult to say how different the coefficients are. In this thesis, the standard deviation of the Seebeck coefficient was large, which shows the importance of including the standard deviation. If Lecce and Bresme have obtained standard deviations of the same order of magnitude as observed in this thesis, the coefficients may be in agreement within the statistical error.

Additionally, the electric field was calculated for the electrolyte solution by summing the mono-, di- and quadrupole contributions to the field. The resulting total electric field was found to be $(-2\pm1)\cdot10^{8}$ Vm^{-1}, where the contribution from the ions was equal to $(3\pm1)\cdot10^{8}$ Vm^{-1} and the contribution from water was equal to $(-4.4\pm0.6)\cdot10^{8}$ Vm^{-1}. The resulting Seebeck coefficient was equal to $(4\pm3)\cdot10^{-3}$ VK^{-1}. Neither the fields nor the Seebeck coefficient were in agreement with the result obtained when the field was calculated from the integral of the charge density, equation (2.28). The total electric field and the Seebeck coefficient even have the opposite sign of the results calculated by Lecce and Bresme [2]. However, the sign of the contribution from the ions and water are in agreement with the results obtained by Lecce and Bresme [2], and in agreement with the results obtained when the field was calculated by integrating the charge density in this thesis.

The average pressure in the electrolyte solution was equal to 678 atm, while Lecce and Bresme used a pressure of 592 atm [2]. The difference in pressure may have influenced the result, and could be an explanation for the missing agreement between the results. Additionally, the system size in this thesis was smaller compared to the system size that Lecce and Bresme used [2]. In the pure water system, the electric fields computed from the different methods were in agreement, and the results were in agreement with the results calculated by Armstrong and Bresme [1]. In the water system, the simulation box was larger, which indicates that a larger simulation box could have given a different result for the electrolyte solution. However, when the field in the electrolyte solution was calculated by integrating the charge density, the electric field was of the same order of magnitude and with the same sign as in the results presented by Lecce and Bresme [2]. There was a larger difference between the results when the field was calculated by summing the mono-, di- and quadrupole contributions to the field, which indicates that the Seebeck effect is a sensitive effect. The

effect became more difficult to capture when the ions were added to water compared to the pure water system.

Another objective of this master's thesis was to investigate if the contribution from the ions to the Seebeck effect in the electrolyte solution depends on the water molecules present in the solution. This was investigated by constructing a system consisting of LiCl, where the dielectric constant for water was used rather than including the water molecules. This is a simplified way of modeling an electrolyte solution. An electric field equal to $(4\pm1)\cdot10^{7}$ V m^{-1} was computed in this system. The Seebeck coefficient was equal to $(-3\pm1)\cdot10^{-3}$ V K^{-1}. The Seebeck coefficient calculated from the integral of the charge density for the electrolyte solution was equal to $(-8\pm3)\cdot10^{-3}$ V K^{-1}, and the ion contribution to the Seebeck effect was found to be $(-1.5\pm0.2)\cdot10^{-2}$ V K^{-1}. These results indicate that the water molecules influences the contribution from the ions to the Seebeck effect. Since it was found for the electrolyte solution that both the contribution from the ions and water need to be taken into account in the calculation of the electric field, it is reasonable that the Seebeck coefficient is different when there are no water molecules present. Additionally, it is expected that there is a larger shielding effect when the water molecules are present compared to when the dielectric constant for water is used, which will influence the charge separation.

Since the results in this master's thesis indicate that the Seebeck effect is a sensitive effect, a systematic study of the pressure and system size dependence of the Seebeck effect is suggested for system number 2 and 3 in table 4.1, in order to gain a better understanding of the role of water in the electrolyte solution. Additionally, it would be interesting to vary the salt concentration, in order to investigate if the difference between the Seebeck coefficients for system number 2 and 3 depends on the salt concentration.

References

[1] Armstrong J, Bresme F. Temperature inversion of the thermal polarization of water. Phys Rev E. 2015;92:060103.

[2] Lecce SD, Bresme F. Thermal polarization of water influences the thermoelectric response of aqueous solutions. J Chem Phys B. 2018;122(5):1662–1668.

[3] Lee SH. Temperature Dependence on Structure and Self-Diffusion of Water: A Molecular Dynamics Simulation Study using SPC/E Model. Bull Korean Chem Soc. 2013;34(12).

[4] Egorov AV, Komolkin AV, Chizhik VI, Yushmanov PV, Lyubartsev AP, Laaksonen A. Temperature and Concentration Effects on Li+-Ion Hydration. A Molecular Dynamics Simulation Study. J Phys Chem B. 2003;107:3234–3242.

[5] Fahrner WR. Semiconductor thermoelectric generators. Trans Tech Publications; 2009.

[6] Kjelstrup S, Bedeaux D. Non-Equilibrium Thermodynamics of Heterogeneous Systems. World Scientific; 2008.

[7] Platten JK. The Soret effect: A review of recent experimental results. J Appl Mech. 2005;73(1):5–15.

[8] Tritt TM. Thermoelectric Phenomena, Materials, and Applications. Annu Rev Mater Res. 2011;41(433).

[9] Vilar JMG, Rubi JM. Thermodynamics beyond local equilibrium. PNAS. 2001;98(20):11081–11084.

[10] Bresme F, Lervik A, Bedeaux D, Kjelstrup S. Water Polarization under Thermal Gradients. Phys Rev Lett. 2008;101(2):020602.

[11] Kjelstrup S, Bedeaux D, Johannessen E, Gross J. Non-Equilibrium Thermodynamics for Engineers. World Scientific; 2010.

[12] Rozmanov D, Kusalik PG. Transport coefficients of the TIP4P-2005 water model. J Chem Phys. 2012;136(4):044507.

[13] Hafskjold B. Computer Simulations of Thermal Diffusion in Binary Fluid Mixtures. In: Thermal Nonequilibrium Phenomena in Fluid Mixtures. Springer; 2002. .

[14] Kjelstrup S, Helbæk M. Fysikalsk kjemi. 2nd ed. Fagbokforlaget; 2006.

[15] Grimnes S, Martinsen OG. Bioimpedance and Bioelectricity Basics. Elsevier Ltd.; 2015.

[16] Atkins P, Paula JD. Physical Chemistry. 10th ed. Oxford University Press; 2014.

[17] Leach AR. Molecular modelling - principles and applications. 2nd ed. Pearson Education; 2001.

[18] Frenkel D, Smit B. Understanding Molecular Simulations. Academic Press; 1996.

[19] Berendsen HJC, Grigera JR, Straatsma TP. The missing term in effective pair potentials. J Phys Chem. 1987;91:6269–6271.

[20] Tuckerman ME. Statistical Mechanics: Theory and Molecular Simulation. Oxford University Press; 2010.

[21] Evans DJ, Morriss GP. Statistical mechanics of nonequilibrium liquids. 2nd ed. ANU E Press; 2007.

[22] Shinoda W, Shiga M, Mikami M. Rapid estimation of elastic constants by molecular dynamics simulation under constant stress. Phys Rev B. 2004;69(13):134103.

[23] Tuckerman ME, Alejandre J, López-Rendón R, Jochim AL, Martyna GJ. A Liouville-operator derived measure-preserving integrator for molecular dynamics simulations in the isothermal-isobaric ensemble. J Phys A: Math Gen. 2006;39(19):5629–5651.

[24] Plimpton S. Fast Parallel Algorithms for Short-Range Molecular Dynamics (`http://lammps.sandia.gov`). J Comp Phys. 1995;117(1–19).

[25] Zumdahl SS, DeCoste DJ. Chemical Principles. 7th ed. Mary Finch; 2013.

[26] Kumar P, Varanasi SR, Yashonath S. Relation between the Diffusivity, Viscosity, and Ionic Radius of LiCl in Water, Methanol, and Ethylene Glycol: A Molecular Dynamics Simulation. J Chem Phys. 2013;117(27):8196–8208.

[27] Iriarte-Carretero I, Gonzalez MA, Armstrong J, Fernandez-Alonsobc F, Bresme F. The rich phase behavior of the thermopolarization of water: from a reversal in the polarization, to enhancement near critical conditions. Phys Chem Chem Phys. 2016;18(29):19894–19901.

[28] Fortran 95 Language Reference;. Available at `www.fortran.com`.

[29] Python Software Foundation. Python Language Reference, version 3.6.4;. Available at `www.python.org`.

[30] Armstrong JA, Bresme F. Water polarization induced by thermal gradients: The extended simple point charge model (SPC/E). J Chem Phys. 2013;130(1):014504.

[31] Armstrong J, Daub CD, Bresme F. Note: How does the treatment of electrostatic interactions influence the magnitude of thermal polarization of water? The SPC/E model. J Chem Phys. 2015;143(3):036101.

[32] Daub CD, Åstrand PO, Bresme F. Thermo-molecular orientation effects in fluids of dipolar dumbbells. Phys Chem Chem Phys. 2014;16(40):22097–22106.

[33] Römer F, Lervik A, Bresme F. Nonequilibrium molecular dynamics simulations of the thermal conductivity of water: a systematic investigation of the SPC/E and TIP4P/2005 models. J Chem Phys. 2012;137(7):074503.

[34] Reddy MR, Berkowitz M. The dielectric constant of SPC/E water. Chem Phys Lett. 1989;155(2):173–176.

[35] Hansen JP, McDonald IR. Theory of simple liquids. 4th ed. Elsevier Science; 2006.

[36] Aylward G, Findlay T. SI Chemical Data. 6th ed. Wiley; 2008.

[37] Vega C, Sanz E, Abascal JLF. The melting temperature of the most common models of water. J Chem Phys. 2005;122(11):114507.

[38] Hens A, Biswaz G, De S. Evaporation of water droplets on Pt-surface in presence of external electric field—A molecular dynamics study. J Chem Phys. 2015;143(9):094702.

[39] Bertolini D, Tani A. Thermal conductivity of water: Molecular dynamics and generalized hydrodynamics results. Phys Rev E. 1997;56(4).

[40] Mills R. Self-diffusion in normal and heavy water in the range 1-45.deg. J Chem Phys. 1973;77(5):685–688.

[41] Vega C, Abascal JLF. Simulating water with rigid non-polarizable models: a general perspective. Phys Chem Chem Phys. 2011;13(44):19663–19688.

[42] Dang LX. Development of nonadditive intermolecular potentials using molecular dynamics: Solvation of Li+ and F ions in polarizable water. J Phys Chem. 1992;96:6979–6977.

[43] Dang LX, Garrett BC. Photoelectron spectra of the hydrated iodine anion from molecular dynamics simulations. J Phys Chem. 1993;99:2972–2977.

[44] Dang LX, Smith DE. Computer simulations of nacl association in polarizable water. J Phys Chem. 1994;100:3757–3766.

[45] Dang LX, Smith DE. Mechanism and thermodynamics of ion selectivity in aqueous solutions of 18-crown-6 ether: A molecular dynamics study. J Phys Chem. 1995;117:6954–6960.

[46] Lorentz HA. Ueber die Anwendung des Satzes vom Viral in der kinetischen Theorie der Gase. Ann Phys. 1881;12:127–136.

[47] Berthelot D. Sur le mélange des gaz. C r hebd séances Acad sci. 1898;126:1703–1855.

[48] Taylor JR. Error Analysis - The Study og Uncertainties in Physical Measurements. 2nd ed. McGuire A, editor. Colorado: University Science Books; 1997.

[49] Adams RA, Essex C. Calculus. 8th ed. Pearson; 2013.

[50] LAMMPS. compute temp/region command — LAMMPS documentation;. (Accessed on 15/03/2018). `http://lammps.sandia.gov/doc/compute_temp_region.html`.

[51] Kreyszig E. Advanced Engineering Mathematics. 10th ed. John Wiley Sons; 2011.

[52] Aragones JL, Vega C. Plastic crystal phases of simple water models. J Chem Phys. 2009;130(24):244504.

A The parameters in the Lennard-Jones potential

In order to model a system consisting of LiCl and water, a potential is needed to describe the interactions between the ions, the interactions between water and ions and the water-water interactions. The potential is given in equation (3.7), and it consists of both Lennard-Jones interactions and Coulombic interactions. The parameters for the SPC/E water model are given in table 3.2. For the ion-ion and ion-water interactions, the model by Dang et al. was used [42–45]. The Li^+-Li^+, Li^+-Cl^- and Cl^--Cl^- interactions are given in table A.1. Additionally, the interactions between the ions and oxygen is given in the table. The interactions between between the ions and hydrogen were neglected because the atomic radius of oxygen and the OH bond length are of equal magnitude [36]. Therefore, the only water-ion interactions included are those between oxygen and the ions.

The parameters for the interactions between lithium and oxygen and between chloride and oxygen are calculated by the Lorentz-Berthelot mixing rules [46, 47]:

$$\sigma_{ij} = \frac{\sigma_{ii} + \sigma_{jj}}{2} \tag{A.1}$$

$$\varepsilon_{ij} = \sqrt{\varepsilon_{ii}\varepsilon_{jj}} \tag{A.2}$$

The parameters for the interactions between Li^+-Li^+, Li^+-Cl^-, and Cl^--Cl^- and for the interactions between the ions and the oxygen are given in table A.1:

Table A.1: The Lennard-Jones parameters, ε and σ, for the ion-ion interactions and the ion-water interactions. The parameters are needed in equation (3.7).

Interaction	ε [kcal mol^{-1}]	σ [Å]
Li^+-Li^+	0.165	1.508
Li^+-Cl^-	0.1000026	2.954
Cl^--Cl^-	0.1000026	4.401
Li^+-O	0.160152	2.337
Cl^--O	0.124684	3.783

B The standard deviation of the mean

The following formula was used for calculating the standard deviation of the mean [48]:

$$\sigma = \sqrt{\frac{1}{N(N-1)} \sum_{i=1}^{N} (x_i - \bar{x})^2}, \tag{B.1}$$

where σ is the standard deviation of the mean, N is the number of samples, x_i represents each value in the population, and $\bar{x}$ is the mean value of the samples. $\bar{x}$ can be expressed as

$$\bar{x} = \frac{1}{N} \sum_{i=1}^{N} x_i \tag{B.2}$$

C Calculation of the cosine to the angle between the dipole vector and the x-direction

$\theta_{\mu x}$ is the angle between the dipole vector and the x-direction. cos($\theta_{\mu x}$) can be calculated from the following formula [49]:

$$\boldsymbol{e_x} \cdot \boldsymbol{e_\mu} = |\boldsymbol{e_x}||\boldsymbol{e_\mu}| \cos(\theta_{\mu x}) = cos(\theta_{\mu x}), \tag{C.1}$$

where **x** is the unit vector in the x-direction

$$\boldsymbol{e_x} = (1, 0, 0) \tag{C.2}$$

and $\boldsymbol{\mu}$ is the unit dipole vector:

$$\boldsymbol{e_\mu} = \left(\frac{\boldsymbol{\mu_x}}{\boldsymbol{\mu}}, \frac{\boldsymbol{\mu_y}}{\boldsymbol{\mu}}, \frac{\boldsymbol{\mu_z}}{\boldsymbol{\mu}} \right) \tag{C.3}$$

where ($\boldsymbol{\mu_x}$, $\boldsymbol{\mu_y}$, $\boldsymbol{\mu_z}$) are the x, y, z coordinates of the dipole vector, respectively. Both |$\boldsymbol{\mu}$| and |$\boldsymbol{x}$|, the lengths of $\boldsymbol{\mu}$ and $\boldsymbol{x}$, in equation (C.1) are equal to 1. This is because $\boldsymbol{\mu}$ and $\boldsymbol{x}$ are unit vectors. $\boldsymbol{\mu}$ is defined as

$$\boldsymbol{\mu} = \sqrt{\boldsymbol{\mu_x}^2 + \boldsymbol{\mu_y}^2 + \boldsymbol{\mu_z}^2} \tag{C.4}$$

Equation C.1 then becomes:

$$cos(\theta_{\mu x}) = \mathbf{x} \cdot \boldsymbol{\mu} = (1, 0, 0) \cdot \left(\frac{\boldsymbol{\mu_x}}{\boldsymbol{\mu}}, \frac{\boldsymbol{\mu_y}}{\boldsymbol{\mu}}, \frac{\boldsymbol{\mu_z}}{\boldsymbol{\mu}} \right) = \frac{\boldsymbol{\mu_x}}{\boldsymbol{\mu}} \tag{C.5}$$

The Python script for calculating the cosine to the angle between the dipole vector and the x-direction is presented in appendix J.2.

D Degrees of freedom in the temperature calculation

LAMMPS computes the temperature by using the kinetic energy according to the following formula [50]:

$$T = \frac{2}{3}\frac{K}{k_B N}, \tag{D.1}$$

where K is the per-atom kinetic energy, N is the number of atoms and k_B is Boltzmann's constant. For water, the fix SHAKE command was used to keep the H-O-H angle and the O-H bonds fixed. This means that 1 degree of freedom is subtracted per atom. The temperature for water should therefore be computed according to the following formula:

$$T' = \frac{2}{2}\frac{K}{k_B N}, \tag{D.2}$$

The relation between the temperature computed by LAMMPS, equation (D.1), and the water temperature, equation (D.2), is equal to:

$$T' = 1.5T \tag{D.3}$$

By setting the target temperature for water in LAMMPS to 2/3 of the actual target temperature, this should yield the correct temperature. I.e. if the target temperature for the hot region is 400 K, the target temperature is set to 2/3·400 K = 266.67 K. In the computation of the temperature profile, the temperature for water was computed according to equation (D.2). The ions present in the electrolyte solution has 3 degrees of freedom, i.e. it is correct to calculate their temperature from equation (D.1). However, in this thesis, only the water molecules in the hot and cold regions were thermostatted to some target temperature. This is because the kinetic energy of the ions in a region will tend to the same kinetic energy as the water molecules in the same region.

E The salt concentration of the electrolyte solution

The salt concentration of the electrolyte solution was equal to 1.01 mol kg^{-1}, as presented in table 4.1.

The salt concentration of the solution is the ratio between the number of moles of LiCl, $\mathrm{n_{LiCl}}$, and the mass of water, $\mathrm{m_{H_2O}}$:

$$\mathrm{c} = \frac{\mathrm{n_{LiCl}}}{\mathrm{m_{H_2O}}} \tag{E.1}$$

The number of moles of LiCl is given by:

$$\mathrm{n_{LiCl}} = \frac{\#\mathrm{molecules_{LiCl}}}{\mathrm{N_A}}, \tag{E.2}$$

where #molecules$_{\mathrm{LiCl}}$ is the number of molecules of LiCl and $\mathrm{N_A}$ is Avogadro's number. The mass of water is given by:

$$\mathrm{m_{H_2O}} = \frac{\#\mathrm{molecules_{H_2O}} \cdot \mathrm{M_{mH_2O}}}{\mathrm{N_A}}, \tag{E.3}$$

where #molecules$_{\mathrm{H_2O}}$ is the number of water molecules and $\mathrm{M}_{m\mathrm{H_2O}}$ is the molar mass of water. By inserting equation (E.2) and (E.3) into equation (E.1), the result is:

$$\mathrm{c} = \frac{\#\mathrm{molecules_{LiCl}} \cdot \mathrm{N_A}}{\mathrm{N_A} \cdot \#\mathrm{molecules_{H_2O}} \cdot \mathrm{M_{mH_2O}}} = \frac{\#\mathrm{molecules_{LiCl}}}{\#\mathrm{molecules_{H_2O}} \cdot \mathrm{M_{mH_2O}}} \tag{E.4}$$

In simulation number 2 in table 4.1, #molecules$_{\mathrm{LiCl}}$=24 and #molecules$_{\mathrm{H_2O}}$=1320, which yields a salt concentration of

$$\mathrm{c} = \frac{\#\mathrm{molecules_{LiCl}}}{\#\mathrm{molecules_{H_2O}} \cdot \mathrm{M_{mH_2O}}} = \frac{24}{1320 \cdot 0.018\,\mathrm{kg\,mol^{-1}}} = 1.01\,\mathrm{mol\,kg^{-1}} \tag{E.5}$$

F Density calculation of simulation number 3

Simulation number 3 in table 4.1 corresponds to the system consisting of LiCl where the dielectric constant for water is used rather than including any actual water molecules. It is important that simulation number 2 and 3 are comparable, since these systems are constructed to investigate if the contribution from the ions to the Seebeck effect in the electrolyte solution depends on the water molecules present in the solution.

The density of simulation number 3 was calculated according to the following formula:

$$\rho[\mathrm{gL}^{-1}] = \mathrm{M_m}[\mathrm{g\ mol}^{-1}] \cdot \mathrm{c}[\mathrm{mol\ L}^{-1}], \tag{F.1}$$

where M_m is the sum of the molar masses of lithium and chloride, which is equal to 42.394 g mol^{-1} and c is the concentration. The salt concentration of simulation number 2 was equal to 1.01 mol kg^{-1} and this corresponds to 0.9997 mol L^{-1}. This means that the density of simulation number 3 should be:

$$\rho = 42.394\,\mathrm{g\,mol}^{-1} \cdot 0.9997\,\mathrm{mol\,L}^{-1} = 42.38\,\mathrm{g\,L}^{-1} = 0.042\,38\,\mathrm{g\,cm}^{-3} \tag{F.2}$$

G Trapezoid rule

When the electric field was calculated by integrating the charge density, equation (2.28), a trapezoid rule was used in order to calculate the integral. The trapezoid rule is a numerical technique for approximating a definite integral. The formula is given by [51]:

$$\int_a^b f(x)dx = \frac{\Delta x}{2}[f(x_0) + 2f(x_1) + 2f(x_2) + ... + 2f(x_{n-1}) + f(x_n)], \tag{G.1}$$

where

$$\Delta x = \frac{b-a}{n} \tag{G.2}$$

and n is sub intervals of equal width.

H Phase diagram for SPC/E water model

The phase diagram for the SPC/E water model obtained by MD simulations was constructed by J. L. Aragones and C. Vega [52].

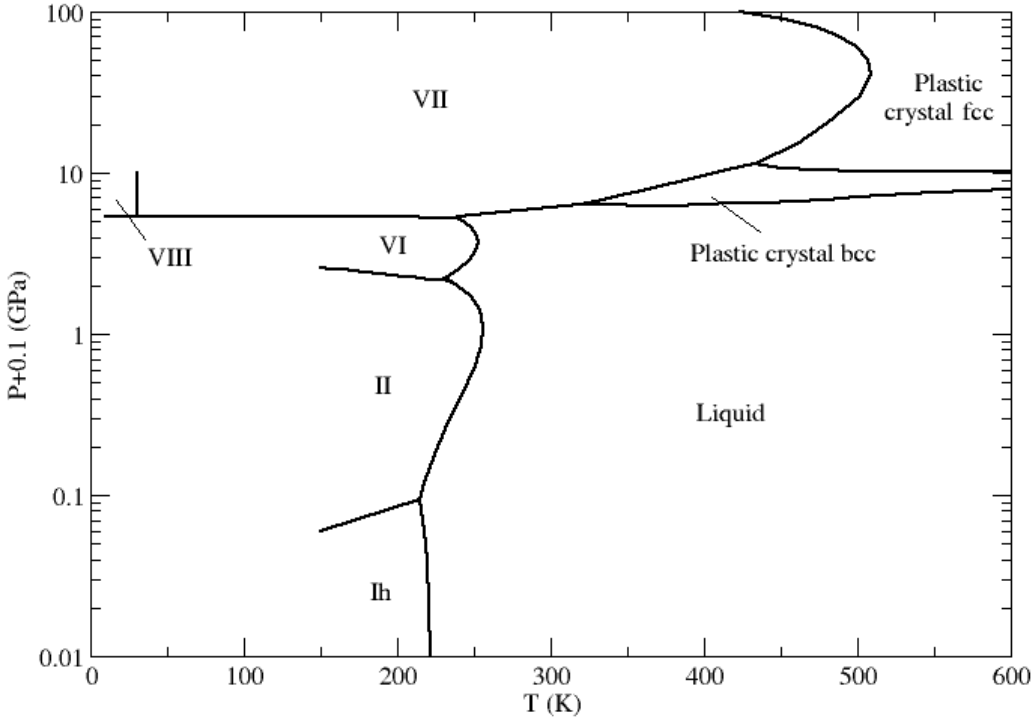

I LAMMPS input scripts

In the following sections, some examples of the input scripts in LAMMPS are given.

I.1 Molecule file for water

The molecule file created for water in LAMMPS.

3 atoms
2 bonds
1 angles

Coords

1 1.55000 2.36649 2.07736
2 1.55000 1.55000 1.50000
3 1.55000 0.73351 2.07736

Types

1 1
2 2
3 1

Charges

1 0.4238
2 -0.8476
3 0.4238

Bonds

1 1 1 2
2 1 2 3

Angles

1 1 1 2 3

Special Bond Counts

1 1 1 0
2 2 0 0

3 1 1 0

Special Bonds

1 2 3
2 1 3
3 2 1

Shake Flags

1 2
2 1
3 2

Shake Atoms

1 1 2
2 2 1 3
3 2 3

Shake Bond Types

1 1
2 1 1 1
3 1

I.2 The NPT simulation for the electrolyte solution

The NPT simulation for the electrolyte solution. This was the first step of the equilibriation.

```
atom_style full
units real

lattice fcc 20
region box block 0 500 0 500 0 500 units box

create_box 4 box bond/types 1 angle/types 1 extra/bond/per/atom 2 extra/angle/per/atom
1 extra/special/per/atom 2

create_atoms 3 random 10 648396 NULL units box

create_atoms 4 random 10 746436 NULL units box

mass 1 1.008
mass 2 15.9994
mass 3 6.941
mass 4 35.453

group Li type 3
group Cl type 4

set type 3 charge +1.0
set type 4 charge -1.0

pair_style lj/cut/coul/long 10
pair_coeff 1 1 0.0 0.0
pair_coeff 1 2 0.0 0.0
pair_coeff 2 2 0.1553 3.166
pair_coeff 3 3 0.165 1.508
pair_coeff 3 4 0.1 2.954
pair_coeff 4 4 0.1 4.401
pair_coeff 1 3 0.0 0.0
pair_coeff 1 4 0.0 0.0
pair_coeff 2 3 0.16 2.337
pair_coeff 2 4 0.125 3.783

bond_style harmonic
bond_coeff 1 0.0 1.0
```

```
angle_style harmonic
angle_coeff 1 0.0 109.47

pair_modify tail yes
kspace_style ewald 1.0E-5

neighbor 2.0 bin
neigh_modify every 1 delay 0 check yes

molecule water in.water
create_atoms 0 random 550 638543 NULL mol water 648376 units box
group H type 1
group O type 2
group vann type 1 2
set type 2 charge -0.8476
set type 1 charge 0.4238

velocity all create 370 648376

fix constrain vann shake 1.0e-4 100 0 b 1 a 1

fix 6 all npt temp 370 370 100 iso 292.15396 292.15396 1000
fix 7 all momentum 100 linear 1 1 1

dump dump all custom 1000 dump.out type id x y z
thermo_style custom step density temp etotal lx press
thermo 1000
run 1000000
write_data data.box
```

I.3 The NVT simulation for the electrolyte solution

The NVT simulation for the electrolyte solution. This was the second step of the equilibriation.

```
atom_style full
units real

pair_style lj/cut/coul/long 10
bond_style harmonic
angle_style harmonic
read_data data.box

replicate 3 1 1

mass 1 1.008
mass 2 15.9994
mass 3 6.941
mass 4 35.453

group Li type 3
group Cl type 4

set type 3 charge +1.0
set type 4 charge -1.0

pair_style lj/cut/coul/long 10
pair_coeff 1 1 0.0 0.0
pair_coeff 1 2 0.0 0.0
pair_coeff 2 2 0.1553 3.166
pair_coeff 3 3 0.165 1.508
pair_coeff 3 4 0.1 2.954
pair_coeff 4 4 0.1 4.401
pair_coeff 1 3 0.0 0.0
pair_coeff 1 4 0.0 0.0
pair_coeff 2 3 0.16 2.337
pair_coeff 2 4 0.125 3.783

bond_coeff 1 0.0 1.0

angle_coeff 1 0.0 109.47
```

```
pair_modify tail yes
kspace_style ewald 1.0E-5

neighbor 2.0 bin
neigh_modify every 1 delay 0 check yes

group H type 1
group O type 2
group vann type 1 2
set type 2 charge -0.8476
set type 1 charge 0.4238

fix constrain vann shake 1.0e-4 100 0 b 1 a 1

fix 6 all nvt temp 370 370 100
fix 7 all momentum 100 linear 1 1 1

dump dump all custom 1000 dump.out type id x y z
thermo_style custom step density temp etotal lx press
thermo 1000
run 1000000
write_data system.box
```

I.4 The equilibriation for the system with LiCl where the dielectric constant for water is used

The equilibriation in the NVT ensemble for the system with LiCl where the dielectric constant for water is used.

```
atom_style charge
units real

lattice fcc 20
region box block 0 120 0 30 0 30 units box
create_box 2 box
create_atoms 1 random 65 64726 NULL units box
create_atoms 2 random 65 53728 NULL units box

group Li type 1
group Cl type 2

mass 1 6.941
mass 2 35.453

set type 1 charge +1.0
set type 2 charge -1.0

pair_style lj/cut/coul/long 10
pair_modify tail yes
pair_coeff 1 1 0.165 1.508
pair_coeff 1 2 0.1 2.954
pair_coeff 2 2 0.1 4.401

kspace_style ewald 1.0E-5
dielectric 51.0
neighbor 2.0 bin
neigh_modify every 1 delay 0 check yes

velocity all create 370 124987
fix 1 all nvt temp 370 370 100

dump dump all custom 1000 dump.out type id x y z
thermo_style custom step density lx ly lz temp etotal press
thermo 1000
```

```
run 500000

write_data system.box
```

I.5 Non-equilibrium simulation for the electrolyte solution

An example LAMMPS script for the non-equilibrium simulation for the electrolyte solution.

```
atom_style full
units real

pair_style lj/cut/coul/long 10
bond_style harmonic

angle_style harmonic

read_data system1.box

mass 1 1.008
mass 2 15.9994
mass 3 6.941
mass 4 35.453

group Li type 3
group Cl type 4
group LiCl type 3 4
set type 3 charge +1.0
set type 4 charge -1.0

pair_style lj/cut/coul/long 10
pair_coeff 1 1 0.0 0.0
pair_coeff 1 2 0.0 0.0
pair_coeff 2 2 0.1553 3.166
pair_coeff 3 3 0.165 1.508
pair_coeff 3 4 0.1 2.954
pair_coeff 4 4 0.1 4.401
pair_coeff 1 3 0.0 0.0
pair_coeff 1 4 0.0 0.0
pair_coeff 2 3 0.16 2.337
pair_coeff 2 4 0.125 3.783

bond_coeff 1 0.0 1.0

angle_coeff 1 0.0 109.47

pair_modify tail yes
```

```
kspace_style ewald 1.0E-5

neighbor 2.0 bin
neigh_modify every 1 delay 0 check yes

group H type 1
group O type 2
group vann type 1 2
set type 2 charge -0.8476
set type 1 charge 0.4238

fix constrain vann shake 1.0e-4 100 0 b 1 a 1

#defining variables
variable d equal xlo
variable e equal xhi
variable Lx equal lx
variable dx equal $Lx/30
variable T1 equal 1*$Lx/30
variable T2 equal 14*$Lx/30
variable T3 equal 16*$Lx/30
variable T4 equal 29*$Lx/30
variable x1 equal $d+$T1
variable x2 equal $d+$T4
variable x3 equal $d+$T2
variable x4 equal $d+$T3
variable Ly1 equal ylo
variable Ly2 equal yhi
variable Lz1 equal zlo
variable Lz2 equal zhi

#creating a temperature gradient
region hot1 block $d $x1 $Ly1 $Ly2 $Lz1 $Lz2 units box
region hot2 block $x2 $e $Ly1 $Ly2 $Lz1 $Lz2 units box
region hot_region union 2 hot1 hot2
region cold block $x3 $x4 $Ly1 $Ly2 $Lz1 $Lz2 units box


# Set up temperature rescale:
compute hot_temp1 LiCl temp/region hot_region
```

```
compute hot_temp2 vann temp/region hot_region

compute cold_temp1 LiCl temp/region cold
compute cold_temp2 vann temp/region cold

fix hot_rescale2 vann temp/rescale 10 300 300 0.0001 1.0

fix_modify hot_rescale2 temp hot_temp2

fix cold_rescale2 vann temp/rescale 10 193.33 193.33 0.0001 1.0

fix_modify cold_rescale2 temp cold_temp2

variable kB equal 0.001987
compute ke_1 LiCl ke/atom
compute ke_2 vann ke/atom
variable T_1 atom (c_ke_1/$kB)*(2/3)
variable T_2 atom c_ke_2/($kB)

fix 7 all momentum 100 linear 1 1 1

# temperature profile
compute chunk all chunk/atom bin/1d x lower $dx units box
fix 8 LiCl ave/chunk 10 100000 5000000 chunk temp v_T_1 file tempprof_ions.out
fix 6 vann ave/chunk 10 100000 5000000 chunk temp v_T_2 file tempprof_w.out

#composition profile
compute H_count H property/chunk chunk count
compute O_count O property/chunk chunk count
compute Li_count Li property/chunk chunk count
compute Cl_count Cl property/chunk chunk count
compute vann_count vann property/chunk chunk count
fix 9 all ave/time 10 100000 5000000 c_H_count c_O_count c_Li_count c_Cl_count
c_vann_count file compprofile.out mode vector

# pressure profile
compute pressure1 all stress/atom NULL
fix dump_1 all ave/chunk 10 100000 5000000 chunk c_pressure1[*] file dump_p.out
norm none

#dipole vector
compute cc1 vann chunk/atom molecule units box
```

compute dipol vann dipole/chunk cc1
fix 10 vann ave/time 100 1 100 c_dipol[*] file dipol.out mode vector

compute 12 vann com/chunk cc1
fix 13 vann ave/time 100 1 100 c_12[*] file com.out mode vector

fix 1 all nve

thermo 1000
thermo_style custom step temp pe etotal press c_hot_temp1 c_hot_temp2 f_hot_rescale2 f_cold_rescale2
dump my_pos all custom 100 dump.lammpstrj mol id type element x y z
run 5000000

write_data system2.box

I.6 Calculation of the self diffusion coefficient for the electrolyte solution

LAMMPS script for calculating the self diffusion coefficients for the electrolyte solution.

```
atom_style full
units real

pair_style lj/cut/coul/long 10
bond_style harmonic
angle_style harmonic
read_data system.box

mass 1 1.008
mass 2 15.9994
mass 3 6.941
mass 4 35.453

group Li type 3
group Cl type 4
group LiCl type 3 4
set type 3 charge +1.0
set type 4 charge -1.0

pair_style lj/cut/coul/long 10
pair_coeff 1 1 0.0 0.0
pair_coeff 1 2 0.0 0.0
pair_coeff 2 2 0.1553 3.166
pair_coeff 3 3 0.165 1.508
pair_coeff 3 4 0.1 2.954
pair_coeff 4 4 0.1 4.401
pair_coeff 1 3 0.0 0.0
pair_coeff 1 4 0.0 0.0
pair_coeff 2 3 0.16 2.337
pair_coeff 2 4 0.125 3.783

bond_coeff 1 0.0 1.0

angle_coeff 1 0.0 109.47

pair_modify tail yes
```

```
kspace_style ewald 1.0E-5

neighbor 2.0 bin
neigh_modify every 1 delay 0 check yes

group H type 1
group O type 2
group vann type 1 2
set type 2 charge -0.8476
set type 1 charge 0.4238

fix constrain vann shake 1.0e-4 100 0 b 1 a 1

fix 6 all nvt temp 370 370 100
fix 7 all momentum 100 linear 1 1 1

compute meansq1 Li msd com yes
compute meansq2 Cl msd com yes
compute meansq3 vann msd com yes

thermo_style custom step c_meansq1[4] c_meansq2[4] c_meansq3[4]
thermo 100
run 2000000
write_data system2.box
```

J Post processing scripts

In the following sections, the post processing scripts are given. The codes are written in Fortran 95 [28] and in Python 3.6.4 [29].

J.1 Python script for the cumulative integration of the charge density

Post processing script for the cumulative integration of the charge density. The trapezoid rule used is presented in appendix G. The code is written in Python 3.6.4 [29].

```
import numpy as np
import scipy.integrate
import os
import sys

def charge(H,O,x):

bins = x.shape[0]
e = 1.602e-19
V = 2788.642826*1e-30
eps = 8.854e-12
rho = (0.4238*(H/V)*e-0.8476*(O/V)*e)/(eps)
print(rho)
E = np.zeros_like(x)
y0 = 1
y1= 25

for i in range(y0+3,y1-2):
E[i-1] = scipy.integrate.trapz(rho[:i],x[:i])


return E

if __name__ == "__main__":

dirName = "6"
INPUT = "2"
fullfile = os.path.join(dirName,INPUT)
data = np.loadtxt(fullfile,skiprows=0)
```

```
chunks = data[:,0]
H = data[:,1]
O = data[:,2]
dx = 2.15724*1e-10
x = np.array([dx*i for i in range(chunks.shape[0])])

E = charge(H,O,x)
print(E)

outputFile = open("ElectricField.out", "w")

for i in range(len(E)):

outputFile.write(str(chunks[i])+" "+str(x[i])+" "+str(E[i])+"\n")

outputFile.close()
```

J.2 Python script for calculating the cosine to the angle between the dipole vector and the x-direction

In the following section, the Python script for calculating the cosine to the angle between the dipole vector and the x-direction is presented. The code is written in Python 3.6.4 [29].

```
import numpy as np
import scipy.integrate
import os
import sys

def calc_dipole():

dipol_chunk_x = np.zeros(len(chunks)-1)
dipol_chunk_y = np.zeros(len(chunks)-1)
dipol_chunk_z = np.zeros(len(chunks)-1)
#av_x = np.zeros(len(chunks)-1)
dipol = np.zeros(len(chunks)-1)
av_cos = np.zeros(len(chunks)-1)
counter = np.zeros(len(chunks)-1)
av_cos = np.zeros(len(chunks)-1)
cos_theta = np.zeros(len(chunks)-1)
## READ DUMP FILE
```

```
for snapshot in range(numSnap):

# read N
_ = inputFile.readline()
_ = inputFile.readline()
_ = inputFile.readline()
line = inputFile.readline()
N = int(line)

# read box dimensions
_ = inputFile.readline()
line_x = inputFile.readline()
line_y = inputFile.readline()
line_z = inputFile.readline()
_boxlo_x, _boxhi_x = line_x.split()
_boxlo_y, _boxhi_y = line_y.split()
_boxlo_z, _boxhi_z = line_z.split()
boxlo_x, boxhi_x = float(_boxlo_x), float(_boxhi_x)
boxlo_y, boxhi_y = float(_boxlo_y), float(_boxhi_y)
boxlo_z, boxhi_z = float(_boxlo_z), float(_boxhi_z)

boxL = np.zeros(3)
hbox = np.zeros(3)
boxL[0] = boxhi_x-boxlo_x
hbox[0] = boxL[0]/2

boxL[1] = boxhi_y-boxlo_y
hbox[1] = boxL[1]/2

boxL[2] = boxhi_z-boxlo_z
hbox[2] = boxL[2]/2

# move forward by one line
_ = inputFile.readline()

snapshots = []
for i in range(N):
line = inputFile.readline()
mol_id, atom_id, atom_type, e, pos_x, pos_y, pos_z = line.split()
snapshots.append([float(mol_id), float(atom_type), float(pos_x), float(pos_y), float(pos_z)])
```

```
tmp_dipole = np.zeros((1,bins))
Hfull = 0
for j in range(1,3600+1):
for snapshot in snapshots:
mol_id, atom_type, pos_x, pos_y, pos_z = snapshot
if (mol_id==j):
if (atom_type==2):
O = [pos_x, pos_y, pos_z]
elif (atom_type==1 and Hfull==0):
H1 = [pos_x, pos_y, pos_z]
Hfull=1
elif (atom_type==1 and Hfull==1):
H2 = [pos_x, pos_y, pos_z]
Hfull = 0

for k in range(3):
if (O[k]-H1[k] > hbox[k]):
H1[k] += boxL[k]
elif (O[k]-H1[k] < -hbox[k]):
H1[k] -= boxL[k]
if (O[k]-H2[k] > hbox[k]):
H2[k] += boxL[k]
elif (O[k]-H2[k] < -hbox[k]):
H2[k] -= boxL[k]

com_x = (Omass*O[0] + Hmass*(H1[0]+H2[0]))/Wmass
com_y = (Omass*O[1] + Hmass*(H1[1]+H2[1]))/Wmass
com_z = (Omass*O[2] + Hmass*(H1[2]+H2[2]))/Wmass

if (com_x > boxhi_x):
com_x -= boxL[0]
if (com_x < boxlo_x):
com_x += boxL[0]
if (com_y > boxhi_y):
com_y -= boxL[1]
if (com_y < boxlo_y):
com_y += boxL[1]
if (com_z > boxhi_z):
com_z -= boxL[2]
```

```
if (com_z < boxlo_z):
com_z += boxL[2]
#print(com_x, com_y, com_z)

for k in range(len(chunks)-1):
if (com_x > chunks[k] and com_x < chunks[k+1]):
dipol_chunk_x[k] = x[j-1]
dipol_chunk_y[k] = y[j-1]
dipol_chunk_z[k] = z[j-1]
counter[k] += 1
dipol[k] += dipol_chunk_x[k]
av_cos = dipol/(counter*0.4893690)
print(av_cos)
return av_cos

if __name__ == "__main__":

bins = 50
numSnap = 20000

Omass = 15.9994
Hmass = 1.008
Wmass = Omass+2*Hmass

x0 = 232.023
dx = 2.15721850512692
x1 = x0+dx/2.0

chunks = [x0+dx*(i) for i in range(51)]
pos = [x1+dx*(n) for n in range(bins)]
#print(len(chunks))
## READ DIPOLE FILE
INPUT = "dipol.out"
for m in range(numSnap):
data = np.genfromtxt(INPUT, skip_header=(4+(3600+1)*m), max_rows=3600)
x = data[:,1]
y = data[:,2]
z = data[:,3]

with open("dump.lammpstrj", "r") as inputFile:
res = calc_dipole()
```

```
outputFile = open("dipol_vector.out", "w")

for m in range(bins):

outputFile.write(str(m+1)+" "+str(pos[m])+" "+str(res[m])+"\n")

outputFile.close()
```

J.3 Fortran script for calculating the mono-, di-, and quadrupole contributions to the electric field

Post processing script for calculating the mono-, di- and quadrupole contributions to the electric field in the electrolyte solution. The code is written in Fortran 95 [28] by Bjørn Hafskjold.

```
program dipole
implicit none
integer,parameter:: n=5010
integer,parameter:: nlayer=32
integer,parameter:: q=60
integer,parameter:: r=4950
integer i,j,jj,k,m,o,p,dummy,step,ntimestep,nreal,nmol,nw,mol(n), &
atom(n),type(n),amol,aatom,atype,counterLi,counterCl,t, &
ionlayer(50000,nlayer), &
ionlayerLi(50000,nlayer),ionlayerCl(50000,nlayer)
real x(n),y(n),z(n),dmoment(r),qmoment(r),dlayer(50000,nlayer), &
qlayer(50000,nlayer), &
xh1,xh2,xo,ax,ay,az,xmin,xmax,xLi,xCl,numLi(q),numCl(q)
character*100 text
character*1 element

open (10,file='dumpfilein',status='old')
open (60,file='dipoles',status='unknown')
open (70,file='quadpoles',status='unknown')
open (20,file='ion',status='unknown')
1000 format (a80)
1010 format (e22.16,1x,e22.16)
1100 format (3i6,3f12.3)
1200 format (4i6,3f12.3)
```

```
1210 format (3i6,a6,3f12.3)
1300 format (f12.3)
1400 format (i6,3f12.3)
1500 format (i6,100f12.3)
1600 format (i6,100i8)

write (*,*) 'Enter number of data dumps'
read (*,*) ntimestep
step=0

5000 continue
step=step+1
if (mod(step,1000).eq.0) write (*,*) step

read (10,1000) text
read (10,*) dummy
read (10,1000) text
read (10,*) nreal
read (10,1000) text
read (10,1010) xmin,xmax
read (10,1000) text
read (10,1000) text
read (10,1000) text

do i=1,nreal
read (10,*) mol(i),atom(i),type(i),element,x(i),y(i),z(i)
enddo

nw=nreal-60
nmol=nw/3

do j=2,nreal
ax=x(j)
ay=y(j)
az=z(j)
amol=mol(j)
aatom=atom(j)
atype=type(j)
do i=j-1,1,-1
if (type(i).le.atype) goto 10
```

```
x(i+1)=x(i)
y(i+1)=y(i)
z(i+1)=z(i)
mol(i+1)=mol(i)
atom(i+1)=atom(i)
type(i+1)=type(i)
enddo
i=0
10 x(i+1)=ax
y(i+1)=ay
z(i+1)=az
mol(i+1)=amol
atom(i+1)=aatom
type(i+1)=atype
enddo

do j=2,nw
ax=x(j)
ay=y(j)
az=z(j)
amol=mol(j)
aatom=atom(j)
atype=type(j)
do i=j-1,1,-1
if (mol(i).le.amol) goto 20
x(i+1)=x(i)
y(i+1)=y(i)
z(i+1)=z(i)
mol(i+1)=mol(i)
atom(i+1)=atom(i)
type(i+1)=type(i)
enddo
i=0
20 x(i+1)=ax
y(i+1)=ay
z(i+1)=az
mol(i+1)=amol
atom(i+1)=aatom
```

```
type(i+1)=atype
enddo

do i=1,nlayer
ionlayerLi(step,i)=0
ionlayerCl(step,i)=0
ionlayer(step,i)=0
enddo

do i=1,nmol
dmoment(i)=0.0
qmoment(i)=0.0
enddo

do i=1,nlayer
dlayer(step,i)=0.0
qlayer(step,i)=0.0
enddo
jj=0

do m=nw+1,nreal
if (type(m).eq.3) then
xLi=x(m)
counterLi=counterLi+1
xLi=(xLi-xmin)/(xmax-xmin)
o=nint(xLi*float(nlayer)+0.5)
if (o.gt.nlayer) o=o-nlayer
if (o.lt.1) o=o+nlayer
ionlayerLi(step,o)=ionlayerLi(step,o)+1
elseif (type(m).eq.4) then
xCl=x(m)
xCl=(xCl-xmin)/(xmax-xmin)
p=nint(xCl*float(nlayer)+0.5)
if (p.gt.nlayer) p=p-nlayer
if (p.lt.1) p=p+nlayer
ionlayerCl(step,p)=ionlayerCl(step,p)+1
endif
ionlayer = ionlayerLi-ionlayerCl
enddo
```

```
do i=1,nw,3
j=i+2
if (type(j).eq.2) then
xo=x(j)
xh1=x(j-2)-xo
xh2=x(j-1)-xo
elseif (type(j-1).eq.2) then
xo=x(j-1)
xh1=x(j-2)-xo
xh2=x(j)-xo
else
xo=x(j-2)
xh1=x(j-1)-xo
xh2=x(j)-xo
endif
dmoment(i)=(xh1+xh2)
qmoment(i)=(xh1*xh1+xh2*xh2)
xo=(xo-xmin)/(xmax-xmin)
k=nint(xo*float(nlayer)+0.5)
if (k.gt.nlayer) k=k-nlayer
if (k.lt.1) k=k+nlayer
if (abs(dmoment(i)).lt.5.0) then
dlayer(step,k)=dlayer(step,k)+dmoment(i)
qlayer(step,k)=qlayer(step,k)+qmoment(i)
endif
enddo

if (step.lt.ntimestep) goto 5000

do i=1,ntimestep
write (60,1500) i,(dlayer(i,j), j=1,nlayer)
enddo

do i=1,ntimestep
write (70,1500) i,(qlayer(i,j), j=1,nlayer)
enddo

do i=1,ntimestep
write (20,1600) i,(ionlayer(i,j), j=1,nlayer)
```

```
enddo

close (10)
close (60)
close (70)
close (80)
close (90)
close (20)
stop
end
```